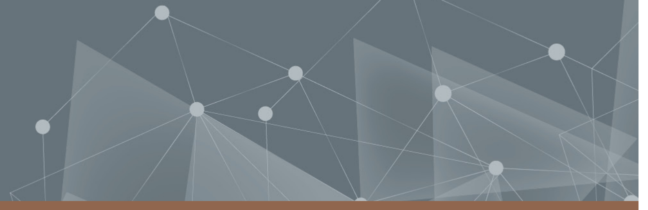

CHALMERS
UNIVERSITY OF TECHNOLOGY

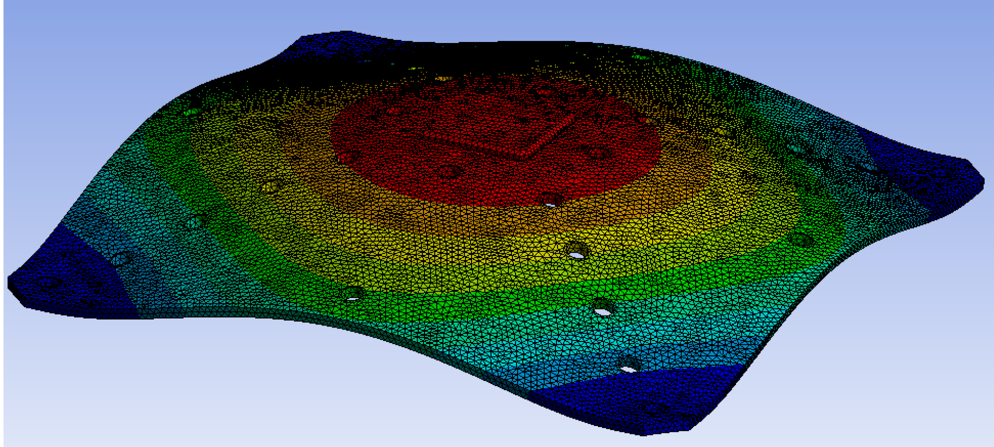

Modelling vibration of printed circuit board assembly to predict component damage

Master's thesis in Applied Mechanics

Filip Lindström
Aron Casen

DEPARTMENT OF MECHANICS AND MARITIME SCIENCES

CHALMERS UNIVERSITY OF TECHNOLOGY
Gothenburg, Sweden 2023
www.chalmers.se

Master's thesis 2023

Modelling vibration of printed circuit board assembly to predict component damage

Filip Lindström
Aron Casen

Department of Mechanics and Maritime Sciences
Division of Dynamics
Chalmers University of Technology
Gothenburg, Sweden 2023

Modelling vibration of printed circuit board assembly to predict component damage
Filip Lindström
Aron Casen

© Filip Lindström, Aron Casen, 2023.

Supervisor: Stefan Högberg, CPAC Systems AB
Examiner: Anders Ekberg, Department of Mechanics and Maritime Sciences

Master's Thesis 2023
Department of Mechanics and Maritime Sciences
Division of Dynamics
Chalmers University of Technology
SE-412 96 Gothenburg
Telephone +46 31 772 1000

Cover: Deformed shape of printed circuit board assembly when subjected to vibrational loading.

Printed by Chalmers Reproservice
Gothenburg, Sweden 2023

Modelling vibration of printed circuit board assembly to predict component damage
Filip Lindström
Aron Casen
Department of Mechanics and Maritime Sciences
Chalmers University of Technology

Abstract

Failure of electronics due to mechanical damage is a prevalent issue in product development. Predicting and preventing failure is difficult without expensive and time consuming physical testing. The aim of this thesis was to develop a model for simulating the mechanical behaviour of printed circuit boards (PCBs). The purpose of the model was to predict the lifetime of ball grid array (BGA) components when subjected to vibration-induced fatigue. The developed model was calibrated based on experimental results, and was able to predict eigenfrequencies, mode shapes and board strains in a satisfactory manner. However, care had to be taken to note whether the relevant deformations were linear or not. If the geometry was nonlinear, this had to be compensated for. Fatigue experiments were also performed with both harmonic and random vibrations, in order to develop a relationship between board strain and number of cycles to failure. Such a relationship, an EN-curve, was established for both harmonic and random vibrations. While these curves can be used to give an indication of a BGA's lifetime, the spread in results is not insignificant. This highlights the difficulties in predicting a lifetime, especially for a new design without experimental data available.

Keywords: FE-model, PCBA, BGA, harmonic vibration, random vibration, solder fatigue, vibration experiments

Acknowledgements

We would like to thank our supervisor Stefan Högberg for his support, advice and insightful discussions. He has also given us many hours of access to the test equipment, allowing us time to perform all the experiments we needed. We also wish to thank our examiner Anders Ekberg for his guidance and feedback, as well as Thomas Abrahamsson for allowing us use of his vibration laboratory at Chalmers University of Technology. Further, the division of failure analysis of electronics hardware at RISE, the research institutes of Sweden, have our thanks for performing the microsectioning analysis, providing us with very valuable insights.

Filip Lindström & Aron Casen, Gothenburg, May 2023

List of Acronyms

Below is the list of acronyms that have been used throughout this thesis listed in alphabetical order:

BGA	Ball Grid Array
CAD	Computer-Aided Design
DAQ	Data Aquisition (System)
DnP	Dye-and-Pry
FE	Finite Element
FEM	Finite Element Method
FFT	Fast Fourier Transform
FRF	Frequency Response Function
HCF	High Cycle Fatigue
LCF	Low Cycle Fatigue
MAC	Modal Assurance Criterion
MAER	Mean Absolute Error, Relative
PCB	Printed Circuit Board
PCBA	Printed Circuit Board Assembly
PDE	Partial Differential Equation
PSD	Power Spectral Density
RMS	Root Mean Square

Contents

List of Acronyms **ix**

1 Introduction **1**
1.1 Aim . . . 1
1.2 Limitations . . . 2

2 Theory **3**
2.1 Electronic components . . . 3
2.2 Modelling of printed circuit board assembly . . . 4
2.3 Vibration studies . . . 4
2.3.1 Modal assurance criterion . . . 5
2.3.2 Finite element method for vibrations . . . 5
2.3.3 Random vibrations . . . 6
2.4 Material fatigue . . . 6
2.5 Accelerometers and strain gauges . . . 7
2.6 Statistical methods . . . 7
2.6.1 Linear regression . . . 8
2.6.2 Bootstrapping . . . 8

3 Method **9**
3.1 Printed circuit board design . . . 9
3.1.1 Soldering process . . . 11
3.1.2 Modelling of geometry . . . 12
3.2 Calibration of material parameters . . . 12
3.3 Vibration experiments . . . 13
3.3.1 Setup . . . 14
3.3.2 Resistance measurements . . . 15
3.4 Numerical evaluation and measurement of acceleration . . . 16
3.5 Numerical evaluation and measurement of strain . . . 18
3.6 Vibration until failure . . . 20
3.6.1 Harmonic vibration . . . 20
3.6.2 Random vibration . . . 21
3.7 Failure analysis . . . 21
3.7.1 Dye-and-pry analysis . . . 21
3.7.2 Microsectioning analysis . . . 22
3.8 Validation . . . 22

3.8.1 Fatigue validation . . . 22
3.8.2 Strain validation of new unit . . . 23

4 Results **25**
4.1 Calibration of material parameters . . . 25
4.2 Modelling of acceleration . . . 27
4.3 Modelling of strain . . . 29
4.4 Harmonic vibration until failure . . . 33
4.4.1 EN-curve . . . 33
4.4.2 Statistical analysis . . . 37
4.5 Random vibration until failure . . . 40
4.5.1 EN-curve . . . 40
4.5.2 Fatigue in middle circuit . . . 41
4.6 Validation . . . 41
4.6.1 Fatigue validation . . . 42
4.6.2 Strain validation of new unit . . . 43
4.7 Failure modes . . . 45
4.7.1 Dye-and-pry analysis . . . 45
4.7.2 Microsectioning analysis . . . 45

5 Conclusion **49**
5.1 Experimental setup . . . 49
5.1.1 Resistance measurements . . . 50
5.2 Spread in results . . . 52
5.3 Model validation versus experiments . . . 53
5.4 Applicability . . . 55
5.4.1 General design tips . . . 55
5.5 Relating random and harmonic vibration . . . 56

Bibliography **59**

1 Introduction

Electronics play a large part in modern vehicles and other machinery. Embedded systems can aid the operator, provide data for diagnostics, and help organise fleets of independent vehicles. Due to the conditions in these machines the electronics often suffer from mechanical damage over time, often caused by vibration. This damage can lead to vital connections being broken, and thus related components failing. The consequences may vary from costs associated with repairs to health risks for operators. All designs must address this problem somehow, or risk an unacceptably short lifetime of the product. Components of the type ball grid array (BGA) are particularly sensitive to vibrations due to their large size and high stiffness [1]. However, it is difficult to predict the performance of a product and where problems can occur. Because of this sensitivity, the use of BGAs has been avoided in safety critical components. However, the functional advantages of BGAs makes such a restriction disadvantageous. The difficulty in prediction also results in situations where the potential problems are being discovered and dealt with late in the product development, when physical prototypes have been produced and tested. This can potentially result in delays and increased costs. If a numerical finite element (FE) model was available to accurately predict the behaviour of a printed circuit board assembly (PCBA) it could be applied early in the process. The data from the FE-model could then be coupled with a predictive model to asses the fatigue life of the solder or other critical parts of the electronics. These aspects combined could provide a useful tool for predicting damage early on in the design process. Furthermore, the intermittent character of BGA failures combined with the need for destructive testing to find the cause of failure makes simulations advantageous, due to the relatively low cost.

1.1 Aim

The aim of the project is to create a general method describing how to simulate the behaviour of a PCBA subjected to vibrational loads in order to predict potential component failure. It is desired that the FE-model computes eigenfrequencies, frequency response functions (FRF) and PCBA strains. This can be compared to threshold values for when a BGA component fails due to mechanical vibration, which are obtained from vibrational experiments. As inputs, the FE-model takes the expected vibrational loads and the geometry of the PCBA. By varying these input parameters, the designer of the PCBA can make an initial design with an

improved chance of fulfilling the required standards. As such, the model serves as an aid when making design choices in the development of the PCBA.

1.2 Limitations

Only mechanically applied vibrational loads are considered in the project. No thermal or other environmental effects are included. This is an important limitation, since it simplifies the analysis. In reality, thermal loads are an important factor in fatigue of electronics [2].

Experimentally, fatigue failure is detected by increase of electrical resistance in the BGA. No other type of damage, such as cracks in the board of the PCBA, are measured. Nor are any other types of components considered, only the BGA is present on the PCBA.

The investigated PCBAs are simplified prototypes, developed solely for this testing purpose. This eliminates some effects that come with a more complex geometry. The quality of the PCBAs is still representative of products in use.

2
Theory

This section discusses theory and previous work concerning several areas of interest for this study. Some aspects that are considered are circuit boards, vibration and fatigue.

2.1 Electronic components

A printed circuit board (PCB) is a board onto which electronic components may be attached in order to connect them in a suitable way. The board with attached components is called a printed circuit board assembly (PCBA). A PCB has several layers, with conductive and insulating materials. The conductive layers contain traces of copper that connect various components on the board. The insulating layers prevent current from flowing in undesired ways, and also provide the major contribution to the PCB's mechanical properties.

A ball grid array (BGA) is a type of component that can be mounted on the surface of the PCB. The purpose of the BGA is to hold a number of integrated circuits, and connect them to the PCB. The bottom side of a BGA is covered in solder balls, each one meant to connect to a corresponding pad on the PCB. The circuits in the PCB then connect each ball to the desired point in the circuit. The distance between the centre of two adjacent solder balls is called pitch, and is constant for any one type of BGA. A finer pitch allows for a more densely populated PCBA, but is less forgiving in manufacturing and soldering. Other properties that may differ between various types of BGA is ball size, number of balls and solder material. Note that the BGA used in this project contains no integrated logic, only connections from one solder ball to the next. This is because the BGA is a dummy component with no function other than being a test specimen for detecting damage.

The insulating layers of a PCB are typically made from FR4-materials, which is a class of glass-reinforced epoxy laminate materials. Such long fiber composite materials have an inherent anisotropy, with different material properties in different directions. Specifically the composites are very stiff and strong in tension along the fiber direction, compared to other directions [3, p.6-7]. FR4 specifically is made from woven glass fibers in an epoxy matrix [4]. Woven composites can be designed to have nearly identical properties in both fibre directions in-plane if desired [3, p.7].

2.2 Modelling of printed circuit board assembly

Modelling a PCBA to predict damage and vibrations has seen success in earlier works. One approach for determining eigenfrequencies is smearing of components, where the properties of the empty board are known, and then altered by components [5] [6]. The added components will increase Young's modulus and density, and alter Poisson's ratio. Smearing is possible to apply locally, if the positions of components are known, or globally if they are not [7]. Smearing is advantageous due to its simplicity. Geometry of components beyond footprint dimensions need not be considered. This also allows the board to be modelled as a 2D-object, meaning that computationally cheap shell elements can be used. While often sufficient for predicting eigenfrequencies, smearing is not ideal for determining stresses and strains, due to the simplification of geometry [6]. Smearing being a viable method indicates that a model does not necessarily need to include all geometric details of components.

Detailed FE models of a PCBA may include fine details on the components, such as individual solder balls on a BGA [8]. The board itself may also be modelled with varied amounts of detail, such as anisotropic properties of layers [9], or details of copper traces. A detailed model is more computationally expensive as well as more time consuming to develop. For a BGA, the strain in the board has been shown to correlate to the stress in the solder balls [8]. Therefore, a simplification that can capture the board strain may be sufficient for damage prediction, even if it does not capture all the finer details of all components.

Despite the composite material's anisotropy, a model can assume identical properties in all directions in plane, so called transverse isotropy. The validity of this assumption is dependent on the material and the desired level of accuracy. Since the in-plane properties play a much larger role than the out-of-plane properties in terms of eigenfrequencies and deformations of a large and thin PCB [9], it may also be sufficient to model the PCB material as isotropic. For this approach to be feasible, the properties in the two in-plane perpendicular directions must be fairly similar, since varying these will have a large effect on eigenfrequencies [9].

2.3 Vibration studies

A mechanical system will have certain special frequencies called eigenfrequencies. Once the system is excited, it may oscillate at these frequencies without further input. If there is a continuous input at an eigenfrequency, the amplitude of the system's response is greatly increased compared to the same level of input at other frequencies. For each eigenfrequency there is also a corresponding mode which describes the motion of the system at the given frequency. The eigenfrequencies and modes are solved for through the eigenvalue problem, where the modes are the eigenvectors and the squared eigenfrequencies are the corresponding eigenvalues.

A mechanical systems typically have some degree of damping. This damping continually dissipates some of the system's energy and stabilizes the oscillations at a maximum value relative to the input accelerations. When the input vibrations stops, the damping eventually causes the oscillation to decay and stop.

2.3.1 Modal assurance criterion

The modal assurance criterion (MAC) is a way of comparing mode shapes. It can be used for comparison between experimentally obtained mode shapes and corresponding simulated mode shapes. For such a study, the modes should closely resemble each other. Let the eigenvectors from the analysis be denoted Φ_{kA} and the corresponding eigenvectors from experiment be denoted Φ_{kX}. To determine how well the eigenvectors correlate, the angle between the analytical and experimental eigenvectors can be computed. For corresponding eigenvectors the angle should be close to zero. The MAC correlation number is the cosine squared of this angle,

$$MAC(i,j) = \cos^2\left(\angle(\Phi_{iA}, \Phi_{jA})\right) = \frac{\left(\Phi_{iX}^T \Phi_{jA}\right)^2}{||\Phi_{iX}||^2 ||\Phi_{jA}||^2}. \tag{2.1}$$

For perfectly correlated modes this becomes one and for orthogonal modes it becomes zero. When stating the MAC-values as a matrix with with simulated and measured eigenfrequencies on the two axes, an ideal correlation has ones along its diagonal. In reality the diagonal elements are unlikely to be identical to one. Values of at least 0.95 indicate close correlation [10, p. 183].

2.3.2 Finite element method for vibrations

For many problems and geometries, the pertinent partial differential equations (PDEs) can not be solved using analytical approaches. Instead, these equations have to be approximated with discretisation methods. The finite element method (FEM) is one approximation method that divides the geometry into small finite regions called elements. These elements can have different geometries depending on the use case. The PDEs can then be solved approximately over these elements using numerical methods.

The mass, stiffness and damping matrices M, K and C are in general numerically assembled. They are square matrices with size $n \times n$ for a system of n degrees of freedoms. The equation of motion can be written as

$$[M]\{\ddot{x}\} + [C]\{\dot{x}\} + [K]\{x\} = \{f\}. \tag{2.2}$$

By introducing the exponential solution $\{x\} = \{X\}e^{i\omega t}$ and solving the eigenvalue problem, the eigenvalues and eigenvectors can be obtained on the format

$$\begin{bmatrix} \omega_1^2 & \cdots & 0 \\ \vdots & \ddots & \vdots \\ 0 & \cdots & \omega_n^2 \end{bmatrix} \text{ and } \left[\Psi\right] = \left[\left\{\psi_1\right\}\left\{\psi_2\right\}\cdots\left\{\psi_n\right\}\right]. \tag{2.3}$$

2.3.3 Random vibrations

When electronics are subjected to vibrational testing, the loads are often applied in a stochastic manner. This is in order to best mimic real world conditions, where vibrations are seldom in the form of pure and steady sine waves [11, p. 188]. For such a vibrational profile, the input can not be described as a simple acceleration for each frequency. Instead, the vibration level is given as a power spectral density (PSD), describing the distribution across frequencies in the unit g^2/Hz. This means that integrating the vibration level along the frequency range gives the root mean square (RMS) acceleration $G_{RMS,in}^2$ input value. For fatigue computations, it may often be more relevant to know the output $G_{RMS,out}^2$. This can be computed at a specific eigenfrequency via the Miles' equation,

$$G_{RMS,out} = \sqrt{\frac{\pi}{2} f_n G Q}, \tag{2.4}$$

where f_n is the eigenfrequency, G is the input PSD vibration in g^2/Hz and Q is the quality factor, a measure of how damped the system is. Since the majority of the damage is caused by cycles of high stress [11, p. 212], the peak value of $G_{peak,out} = G_{3\sigma} = 3G_{RMS,out}$ is often used.

2.4 Material fatigue

High cycle fatigue (HCF) is characterised by a high number of cycles consisting of mostly elastic deformations. The number of cycles to failure in HCF is typically 10^4 or more. Under HCF conditions, a crack is initiated at some point during loading, and then propagates slightly for each cycle. In vibrational loading, each period of the load is one cycle, and since frequencies may be in hundreds or thousands of Hz, HCF is necessary if the loads are applied for anything more than very short time periods.

The fatigue characteristics of a given material may be presented by an SN-curve, exemplified in figure 2.1. In such a curve, each stress amplitude corresponds to a number of cycles to failure. This assumes a constant amplitude of stress cycles for the entirety of a specimen's life. As in figure 2.1, the SN-curve may often be linearised in the HCF region for simplified analytical estimations, but this is not a requirement. Some materials also exhibit a fatigue limit, where stresses below a certain level do not cause any damage at all [12, p.501-502]. If a material behaves linear elastically there is a simple one to one conversion between stress and strain. The standard SN-curve may then be translated into an equivalent EN-curve, where stress is replaced by strain.

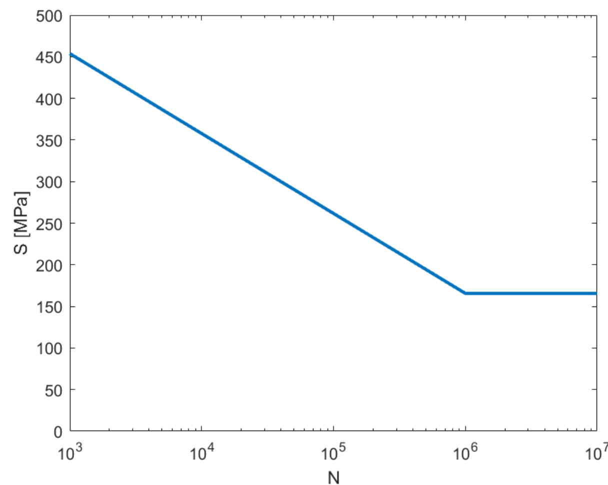

Figure 2.1: Example of an SN-curve describing how the number of cycles to failure varies for different stress levels.

In contrast to HCF, low cycle fatigue (LCF) is characterised by plastic deformations in each cycle, and lives shorter than 10^4 cycles. In this realm a strain based approach is typically superior to a stress based one. This method is different from simply translating the stress in an SN-curve to a strain.

2.5 Accelerometers and strain gauges

An accelerometer is used to measure acceleration, typically in one or several distinct directions. The type of accelerometer used in this project uses a mass-spring system connected to a piece of piezoelectric material. When an acceleration acts upon the mass, the resulting displacement can be correlated to a specific acceleration value. The piezoelectric material is set up to be subjected to the same displacement. Since the material is piezoelectric, a deformation results in an electric signal. Thus, a correlation between acceleration and output voltage can be established.

A strain gauge is an instrument used to measure strain on the surface of an object. The strain gauge is constructed in such a way that its electrical resistance changes as it deforms [13, p. 19]. The time history of the strain can therefore be obtained by continually monitoring the resistance of the gauge. The resistance is typically measured using a Wheatstone bridge [13, p. 147]. Like for accelerometers, the relationship between strain and resistance is unique to each individual strain gauge.

2.6 Statistical methods

To properly describe and discuss experimental results, statistical methods are needed. The most important ones for this study is linear regression and bootstrapping.

2.6.1 Linear regression

In order to produce a linear curve from scattered data points a linear regression method can be applied. Two different methods are used in this study, a standard least square method and a Theil-Sen method.

The least squares method computes the line that minimises the sum of squared distances between data points and line. Due to the squaring of the error, any outliers in the data set have a large effect on the result. The resulting linear function may be analysed via its mean absolute error (MAE), which is computed as

$$MAE = \frac{1}{n}\sum_{i=1}^{n}|y_i - \hat{y}_i|, \tag{2.5}$$

where n is the total number of points in the fit, y_i is the value of the data points and $\hat{y}_i$ is the value of the linear fit at the same x-position. In order to compare fits with different scales on the y-axis, the MAE-value can be divided by a mean y-value, $\bar{y}$. This converts the MAE to a relative error, MAER,

$$MAER = \frac{MAE}{\bar{y}}. \tag{2.6}$$

In order to evaluate the influence of outliers, the Theil-Sen estimator can be used. This linear regression method computes the slope and intercept for all pairs of points, and gives the median values as the result. This means that how much an outlier differs from the expected result is not important, only the number of outliers. In this sense, the Theil-Sen method is more robust than least squares.

2.6.2 Bootstrapping

Bootstrapping is a method for analysing the distribution of data. In this case, with a sample size of n points, a number of data sets each also consisting of n points is constructed. Each such new set contains a random sampling of points from the original set, with the possibility of a point being included more than once. For each such new set of data, a linear regression can be performed in the same way as for the original data set [14]. Thus bootstrapping allows for an analysis similar to if there were more data points available than there are in reality. By analysing the distribution of resulting line slopes and intercepts, an indication of the spread and sensitivity of results can be obtained. If the spread in slopes of bootstrap sets is large, the linear fit is likely to be sensitive to which points are or are not included.

3
Method

To simplify both the testing procedure and the simulations, a special PCBA was designed for this project. It consists of one BGA component centered on a PCB with multiple fastening holes symmetrically distributed around the BGA. This allowed for a variety of fastening points in order to excite different vibrational modes of the PCBA. The BGA was of daisy-chain type and the connectors in the PCBs were designed such that a circuit was created through all soldering points in the PCBA.

An FE-model corresponding to the PCBA was developed. In particular, it was suitable for capturing the dynamic response of the board when subjected to vibrational loading. In order to calibrate the FE-model towards the produced test boards, the FRF of the FE-model was compared with an experimentally obtained FRF for the test board.

The aim of the experiments was to determine two things. Firstly, the behavior of the board when subjected to vibrational load in terms of strain and acceleration at the location of the BGA. This was determined with the use of strain gauges and accelerometers. It enabled tuning of the FE-model, making sure it could capture the response in the same way as the experiments. Secondly, fracture of the solder material on the BGA had to be detected by measuring the resistance through the daisy-chain. A resistance twice as large as the initial value was set as the threshold value indicative of fracture [8]. The experiments were performed at predetermined acceleration levels to establish a correlation between PCB-strain and cycles to failure. From this data a damage measure was devised, predicting failure based on strains levels at the BGA-position [8].

3.1 Printed circuit board design

The PCB-design was developed solely for this project. The design is shown in figure 3.1. The BGA component has a side length of 17 mm and a pitch of 1 mm in each direction. As can be seen from the figure, the BGA is to be soldered at the middle of the PCB. Pin-outs were created at the top right to enable resistance monitoring over the soldering balls. Several symmetric holes were added for mounting the PCB onto the fixture using small M3 standoffs. The hole-pattern is numbered from one to seven to easily describe the mounting-setup. The thickness of the PCB was chosen to 1.6 mm, which is around the typical PCB thickness at CPAC Systems AB. The

size of 108×108 mm was chosen to give a reasonable distance between the standoffs and the BGA component. The PCBs were manufactured of FR4 substrate material with an electroless nickel gold coating, which is suitable for mounting of BGAs.

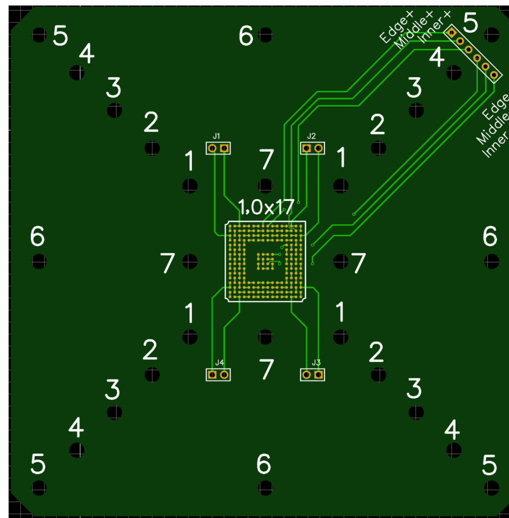

Figure 3.1: Top view of the PCB without BGA attached. The design of the PCB was made such that three circuits were created for resistance monitoring.

Figure 3.2 shows the ball layout of the component, which has four rows of soldering balls along the circumference and 4 × 4 balls in the middle. These 208 balls were divided into three different circuits, highlighted by the three different colours. The resistance in each circuit was monitored individually during the experiments. The first circuit is the outer row, shaded with yellow in figure 3.2. The middle circuit is shaded with red and the inner circuit is shaded with blue. The component is of type daisy-chain, which means that a continuous circuit is created through all soldiering balls in each circuit. This is explained by figure 3.3, that shows a section cut of the PCBA. The balls in the BGA are connected pairwise. By connecting the right soldering balls to the PCB a continuous circuit is created. A possible damage in one of the soldering balls was detected as a sudden increase in resistance, which was captured by the experimental setup, see section 3.3.2. Due to the different circuits, it was clear if the damage was in the outer zone, the middle zone or the inner zone, described by figure 3.2. However, without further investigation, no conclusion could be drawn of exactly which soldering was damaged in the circuit. Nor was it possible to determine whether the damage had occurred in the soldering or due to internal cracks in the copper traces inside the PCB.

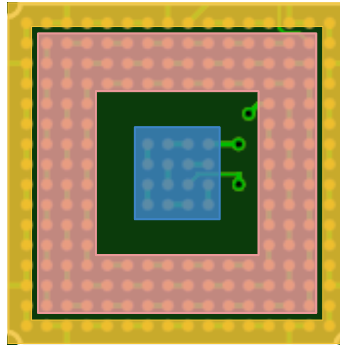

Figure 3.2: The three zones corresponding to the outer, middle and inner circuits, marked in yellow, red and blue.

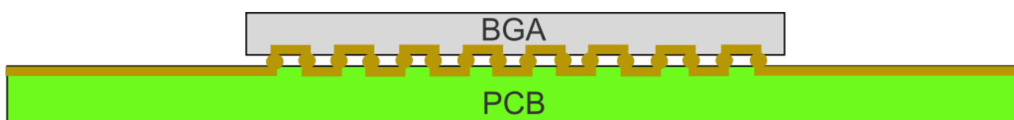

Figure 3.3: The component is of daisy-chain type such that a circuit was created through all of the soldering balls.

3.1.1 Soldering process

The soldering process is an important part of the PCBA manufacturing since it is in the soldering that the fatigue failure will most probably occur first. To get a representative and useful fatigue study, it is crucial that the soldering was done with the same procedure and quality as all other products at CPAC. Therefore, the PCBA assembling was outsourced. The whole process was done in a fully automated surface mounting line. The procedure started by lining up the PCB underneath a solder paste stencil to apply SAC305 solder paste onto the soldering points. Then the BGA component was placed onto the PCB with a camera controlled pick-and-place robot to guarantee perfect positioning. The boards were then heated in a controlled oven to give the correct temperature behaviour for the soldering. The temperature evolution over time is given in figure 3.4.

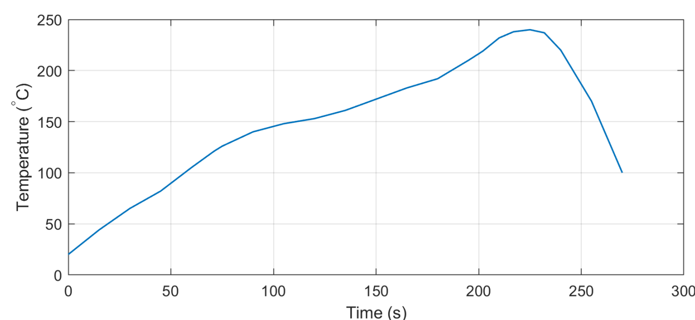

Figure 3.4: Oven temperature as a function of time during the soldering process.

3.1.2 Modelling of geometry

To perform numerical FE-simulations of the PCBA, a CAD-model was created with all the geometrical dimensions of the PCB. Some simplifications were performed in order to create efficient simulations. Therefore, all the soldering balls of the component were neglected. Instead the component was modelled as a homogeneous plate assembled to the PCB. The size and height of the plate corresponded to the real size of the component. Whenever an acceleration sensor was added onto the PCB, a point mass m_{acc} was added to the CAD-model in the corresponding position.

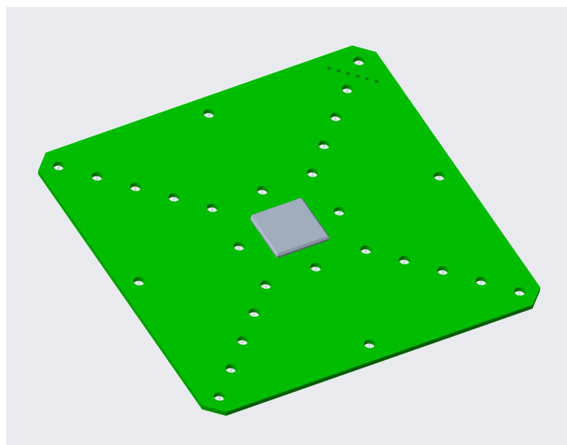

Figure 3.5: CAD model of PCBA, with the component simplified to a homogeneous solid of correct size assembled to the PCB.

3.2 Calibration of material parameters

To compensate for possible deviations in geometry and material properties between the CAD model and reality, a calibration of material parameters was performed. The parameters varied were the Young's modulus of PCB and BGA, damping factor of the system and mass of accelerometers. This calibration required physical testing to find eigenfrequencies and eigenmodes of the PCB, both with and without component soldered to the PCB. Comparing the simulations to the experiment while varying the material parameters enabled calibration.

To find the physical FRFs, six accelerometers were placed onto the PCBA as shown in figure 3.6. These positions were strategically chosen to capture the six first elastic eigenmodes. The PCBA was hung in thin lines to minimise the effect from the surroundings. To excite the modes, the PCBA was hit with a hammer while the vibrations were logged. An average of five hammer hits were used to compute the FRFs for all six channels.

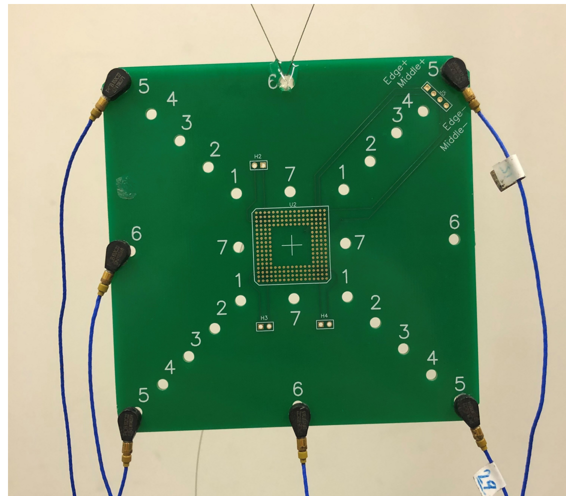

Figure 3.6: Experimental setup for calibration. The PCB was hung in thin lines with six accelerometers measuring the vibrations from hammer hits.

In the FE-model, local coordinate systems were placed in the six sensor positions shown in figure 3.6. Point masses were added at the sensor positions to represent the mass from the sensors. The simulated movements in the local coordinate systems were obtained from the solution. The density was set fixed to $1950\,\mathrm{kg/m^3}$ for both PCB and BGA component. This density was computed by physically weighing the PCBA and dividing its mass by its volume from the CAD-model. The mass of the accelerometers was measured to be $1\,\mathrm{g}$. However, since each accelerometer also has a length of cable attached the mass of the accelerometers was also included as a parameter.

By evaluating the MAC-correlation for different combinations of material parameters, the model could be calibrated to better fit the test data. This was done for Young's modulus E when the PCBA was regarded as one homogeneous material and for the weight m_{acc} of the accelerometers. The optimal parameters are fully presented in section 4.1. It turned out that Young's modulus E only had a small effect on the mode shapes of the PCBA.

On the other hand, E had a large impact on the eigenfrequencies for the first five vibrational modes. The value of E was therefore calibrated to make eigenfrequencies match, rather than modes. The least square method was used to compute the deviation in eigenfrequency. This comparison was made both for the case of empty PCB and for the assembled PCBA. The model was calibrated further by introducing the stiffness of the component as an individual parameter E_{BGA}. The complete list of material parameters and calibrated values are given in table 4.2.

3.3 Vibration experiments

The bulk of experimental work was in the form of vibrational experiments. In general, the experiments were divided into two categories with two different purposes.

The first purpose was to calibrate and validate the FE-model. With the same setup in experiments and simulation, the results of the simulated PCBA behaviour should be as closely correlated as possible to reality. Therefore, the PCBAs were vibrated under certain controlled inputs and the behaviour of the PCBAs were continuously measured. The quantities of interest were the component acceleration and PCBA strain to which the component was exposed. With this data, it was possible to check how well the simulations in section 3.4 coincided with reality.

The second purpose of the vibrational experiments was to establish a relation between the board strain of the PCBA and the cycles to failure. For this reason, the PCBA was vibrated until cracks occurred in the soldering. The calibrated FE-model was used to simulate the PCBA strain underneath the BGA component. The cracks in the soldering were detected by continuously measuring the resistance through all soldering points. Sudden increases in resistance is typical for a glitching soldering.

3.3.1 Setup

The setup of the vibrational experiments involved a lot of different equipment. For a good overview of the different parts in the setup, it is schematically sketched in figure 3.7. The centerpiece of the vibrational experiments was the electromagnetic shaker which was used to excite the test object with a variety of vibrational patterns. The shaker is controlled by a PC through a data acquisition system (DAQ) and a power amplifier. The PC-program sets the specific vibrational pattern and the DAQ makes sure to adjust the power to the shaker to maintain the correct vibrational pattern. To be able to do this the DAQ requires control accelerometers measuring the vibration of the fixture.

The purpose of the fixture was to be an adapter between the shaker and the PCBAs. It had multiple threaded holes to match all the stand-off holes in the PCBAs. The fixture had to be rigid enough not to introduce any undesirable natural frequencies that affected the PCBAs. The PCBAs were mounted to the fixture with M3 standoffs. Two accelerometers were placed onto the fixture for controlling the vibration and a smaller accelerometer was placed underneath the BGA component in the center of the PCBA. This smaller accelerometer was used for measuring the amplified acceleration of the PCBA and had no impact on the control of the shaker. A strain gauge-rosette was also attached to one of the PCBAs to measure the board strain at the corner of the component. See section 3.5 for a more detailed description. A resistance measuring device was also connected to the PCBAs for logging the resistance through the circuits. The resistance measuring is described in section 3.3.2.

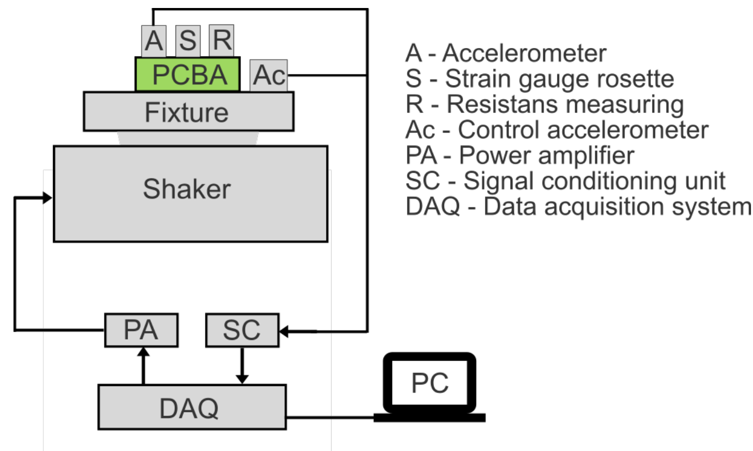

Figure 3.7: Setup of equipment during vibrational experiments.

3.3.2 Resistance measurements

In order to detect failure in the solderings of the component, the resistance in the circuits was continuously monitored using an Arduino Micro. The set-up is described in figure 3.8 with the Arduino represented by the grey box. From the 5 V pin, one of the PCBA circuits was connected in series with a 82 Ω resistor. The PCBA-resistance and the first 82 Ω resistor is denoted R_1. Pin $A0$ measured the voltage U_{A0} over R_1. The second resistor $R_2 = 82\,\Omega$ connected the $A0$ pin to ground. With this setup, the unknown resistance R_1 could be computed as

$$R_1 = R_2 \left(\frac{5\,\mathrm{V}}{U_{A0}} - 1 \right). \tag{3.1}$$

This circuit was repeated on all twelve analog pins on the Arduino, meaning that the resistance could be monitored in up to twelve PCBA-circuits individually at all times.

An important part of the resistance measuring was to have a high sampling rate of the measurements in order to capture glitching in the soldering. The computation of the resistance in the Arduino was faster than the transfer rate of the USB-cable to the computer. Therefore, the Arduino made ten discrete resistance measurements and averaged them before sending the averaged resistance to the PC. In order to improve the sampling rate, only three pins were used on the Arduino, rather than twelve. Approximately 1500 measurements on each of the three channels were performed every second. If one of the ten measurements showed discontinuity in the circuit, the average was marked as discontinuity. Since the highest relevant eigenfrequency was found to be 826 Hz, see table 4.4, this sampling rate was deemed high enough to be able to capture glitching as it occurs.

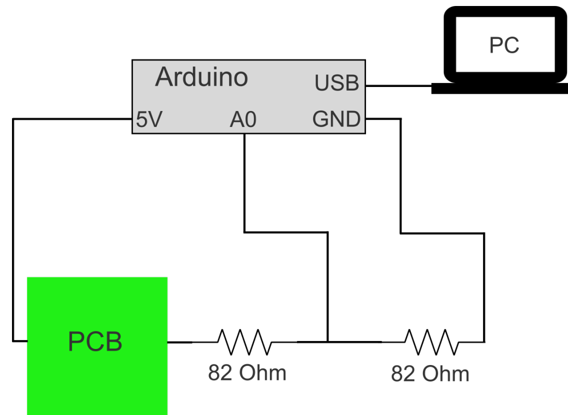

Figure 3.8: Schematic description of voltage divider circuit for resistance measurements.

3.4 Numerical evaluation and measurement of acceleration

When the PCBA was connected to the fixture and vibrated at a certain acceleration level, the BGA component in the center of the PCBA was sometimes exposed to a higher acceleration, depending on the mode shape. The mode shapes are highly dependant on which fastening points are used for the PCBA. To investigate this relation further, a sine sweep from 10 to 1000 Hz was performed experimentally and simulated using Ansys Mechanical. The acceleration level was set consistent at $0.1\text{g} = 0.982\,\text{m/s}^2$ on the entire frequency spectrum. The primary eigenfrequency for each hole fastening was found as the frequency with the largest response accelerations. In the simulations, the accelerational response was measured in the same position as in experiments and the sensor was represented using an added point mass of 1 g.

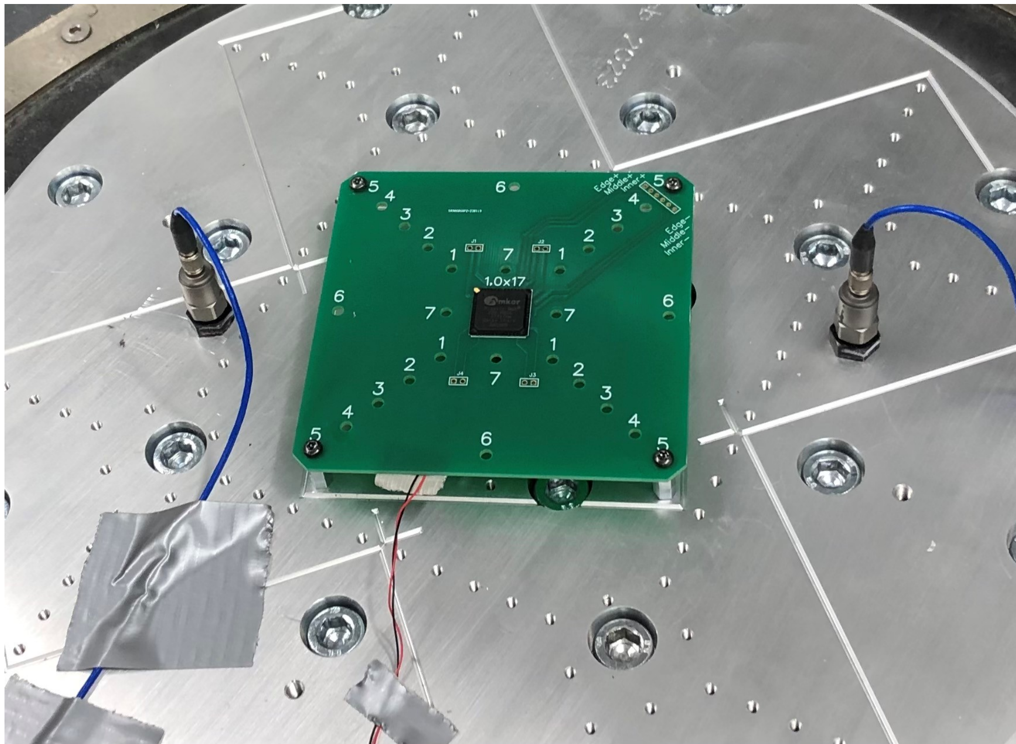

Figure 3.9: PCBA mounted to the fixture, in this case using hole fastening 5. Two accelerometers were used to control the vibration and one small accelerometer was mounted underneath the component.

The simulations were performed using the harmonic response toolbox. The acceleration was applied in the fastening points to simulate the vibration of the fixture. The results from the simulations and experiments were compared in order to establish a damping factor in the PCB and a feasible way of modelling the fastening points.

An important part in the modelling procedure was to determine how to define the boundary conditions of the model. In this case, this corresponds to modelling the fastening of the PCBA. In the experiments, the PCBA was screwed in place using M3 screws into M3 standoffs, see figure 3.9. Four different ways of modelling this were investigated, by fixing different areas around the holes, as displayed in figure 3.10. The red colour represents the surfaces that are fixed in the model for the different simulations. For the first simulation, only the inside of the holes were fixed. For the second case, both the inside and the surfaces beneath the screw were fixed, while case 3 and 4 only had the top and bottom surfaces fixed. For case 2 and 3 the fixed surface had a diameter of 5 mm while case 4 had a diameter of 4 mm. In order to decide which method to use, the simulated eigenfrequency for the primary mode was compared to the corresponding experimental eigenfrequency. This was done for four out of the seven different hole fastenings. The chosen hole fastenings were the ones where one mode greatly amplified the acceleration in the middle of the PCBA.

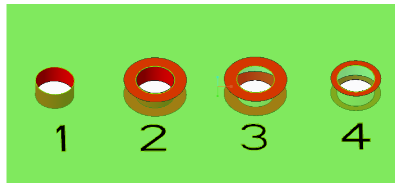

Figure 3.10: Different ways of modelling the boundary conditions at the fastening points.

In order to match the peak values of response acceleration a damping factor had to be calibrated. Literature suggest a damping factor of $0.1 - 2\%$ depending on a variety of factors [15]. Some initial trial and error indicated that the damping ratio of the studied PCBAs should be around $0.4 - 0.5\%$. This was investigated further by comparing the maximum simulated acceleration to the maximum measured acceleration at the primary eigenfrequency. This was done at the same four hole fastenings as before and repeated with damping factors of 0.4, 0.45 and 0.5%.

3.5 Numerical evaluation and measurement of strain

Given a certain value of the acceleration at a certain hole-combination, it is of interest to know the strain in the PCBA. During experiments, the strain could be measured using strain gauge rosettes glued to the PCBA. These give local information about the strain in three different directions. Since strain gauges can not be removed after they are glued to a surface, the strain measuring was restricted to one PCBA. The PCBA strain was evaluated using FE-simulations and compared with corresponding experiments. Verification of strain-simulations was also important to evaluate if the experiments could be replaced by simulations in future work.

Previous experiences at CPAC Systems indicated that the corner solderings of the BGA are exposed to the highest strain levels. Gold plated surfaces were therefore prepared on the backside of the PCB, underneath the component corners. These surfaces are suitable for applying a strain gauge and can be seen in figure 3.11. The right figure shows a strain gauge rosette glued to the PCB. It measured the strain in three directions, marked with the black arrows in the figure. The strain was measured during a sine sweep from 10-1000 Hz at several specific acceleration levels. Repeating these measurements gave a relation between maximum PCBA strain and accelerational level for each hole fastening. The strain was numerically evaluated as the average strain on a 1×1 mm square precisely underneath one of the corner solderings of the BGA. It was necessary to use an averaged measure instead of finding the maximum value due to strain concentrations at specific nodes.

After each measurement the time history of strains measured by the strain gauge was exported to MATLAB for processing. Due to noise in the signal, filtering was necessary to retrieve relevant strain values. The noise was most prominent at a frequency near 50 Hz and multiples thereof. This indicates that the noise is a result

of electrical disturbances, rather than actual variations in strain. A Butterworth filter was applied to the signal for each such potential noise frequency in the relevant range, $10 - 1000\,\text{Hz}$. To this filtered signal, a fast Fourier transform (FFT) was applied. The FFT transforms the signal from the time domain to the frequency domain, which confirmed that the peak strain occurred at roughly the same frequency as the peak acceleration. Once this frequency was computed, the raw data was filtered using a bandpass filter, filtering all frequencies except the peak $\pm 1\,\text{Hz}$. By the use of this filtering process, the amplitude of the strain at the peak response acceleration could be evaluated.

Due to geometric non-linear effects that the FE-model did not account for, the numerically evaluated strains differed from the experimental values for high acceleration levels. Therefore, a method to compensate for this difference was devised. This method was based on identifying a break point between the linear and non-linear regions of the strain-acceleration curve. The curve was then assumed to be behave linearly also for accelerations higher than the break point, but with new slope and intercept values. A rule of thumb was devised for computing the break point based on the deformation angle, and adjusting the slope of the linear curve at this point. For a PCBA with a maximum out-of-plane deformation z, and a distance d between the point of this maximum deformation and the closest fastening point, the deformation angle θ is defined as

$$\theta = \arctan \frac{z}{d}. \tag{3.2}$$

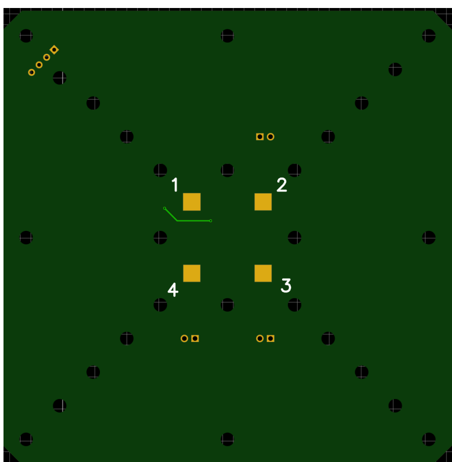

(a) PCB design

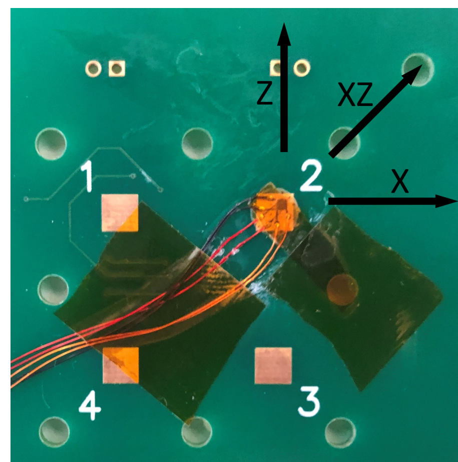

(b) Glued strain gauge

Figure 3.11: The left figure shows gold-plated surfaces that were prepared on the backside of the PCB to fasten strain gauge rosettes. The right figure shows a strain gauge rosette glued to the second position. It measured strain in three directions.

3.6 Vibration until failure

By vibrating the PCBAs until failure occurs, it is possible to evaluate the fatigue characteristics for the solder joints. For high cycle fatigue, this is normally presented by an SN-curve where each stress level in the solder joint corresponds to a number of cycles to failure. However, since the stress in the solder joint is difficult to measure experimentally, an SN-curve could not be obtained directly. Instead, the PCBA strain was related to the number of cycles to failure. To verify this method, an FE-model was used to simulate both the solder joint stress and the PCBA strain for different acceleration levels at the first eigenfrequency. In this FE-model, the full geometry of the component was used with all 208 solder balls. The stress was taken as the average of the first principal stress in one of the corner balls and the strain was taken as the average of the first principal strain in the PCBA board underneath the corresponding component corner. As can be seen from figure 3.12 the solder stress and board strains are linearly correlated, which justifies the use of an EN-curve with the board strain rather than strain or stress in the solder itself. The relation was established for four different hole fastenings of the PCBA. The results are similar which means that a specific board strain can be correlated to a specific solder stress level regardless of the hole fastening in use.

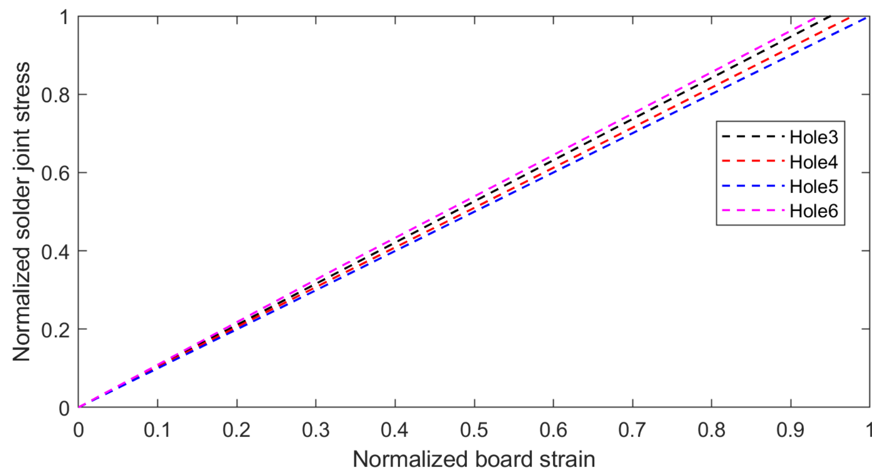

Figure 3.12: Relationship between the maximum PCBA strain and maximum corner solder stress.

3.6.1 Harmonic vibration

To determine the EN relation between cycles to failure and strain levels, the PCBAs were vibrated at specific acceleration levels until failure. Four different hole combinations were used (3, 4, 5 and 6). Before each PCBA was subjected to severe vibration, a sine sweep was performed at 0.1 g near the eigenfrequency found in table 4.3 to determine the exact eigenfrequency of this specific board. These frequencies varied slightly between PCBAs. The PCBA was then vibrated at a higher constant acceleration, $4.5 - 11$ g, sweeping around the eigenfrequency with 1 Hz

on each side. This acceleration level was then maintained until failure in a circuit was detected, through the resistance monitoring discussed in section 3.3.2. From each such experiment, the strain was computed based on the acceleration and hole-fastening.

3.6.2 Random vibration

Fatigue during random vibration was also investigated.The experiments were performed with the same setup as previously discussed, but with a random vibration profile. The profile was of constant PSD level over the interval of 10 to 1000 Hz and constant during the course of any one experiment until failure occurred. The accelerational level was changed between different experiments in the interval of 0.13 to 0.5 g^2/Hz depending on the hole fastening used. The resistance through the PCBA was monitored in the same way as before.

In order to produce an EN-curve for these random vibration experiments, a measure of strain had to be developed. This was done by computing the equivalent $G_{3\sigma,out} = 3G_{RMS,out}$ acceleration value at the most severe eigenfrequency of each board. Here, Miles' equation, (2.4), was used, with the value $Q = 111$ computed using the half-power bandwidth method on the response acceleration. This $G_{3\sigma,out}$ value was then converted to an equivalent $G_{3\sigma,in}$ at the specific frequency via the measured acceleration amplification, which was in turn converted to a strain $\epsilon_{3\sigma}$ using the rule of thumb discussed in section 3.5.

3.7 Failure analysis

Due to the solderings being located between the BGA and PCB, inspection and failure analysis of solderings is mostly dependent on destructive testing. The two methods applied were dye-and-pry (DnP) and microsectioning.

3.7.1 Dye-and-pry analysis

In order to inspect the solder balls after failure, a DnP analysis was applied to a failed PCBA. First, the PCBA was cleaned using isopropyl alcohol, removing dirt and excess flux from the soldering process. A dye was then carefully applied around the edges of the BGA, and care was taken to note whether the dye could enter the gap between BGA and PCB on all sides. Next the entire PCBA was submerged in the dye, and was flexed very slightly, allowing further penetration of the dye in existing cracks. While still submerged in the dye, the PCBA was then placed in a vacuum chamber for approximately 30 minutes. This increases the likelihood of the dye penetrating cracks of smaller sizes. The PCBA was then placed in an oven and heated to 80 °C for several hours, allowing the dye to dry.

Once the dye had been properly dried, the BGA was pried off of the PCB. By inspecting the BGA and PCB in a microscope, cracks in the solder could be identified, since any crack present during dying should ideally be clearly colored red. This

allowed identification of each individual damaged solder ball, unlike the resistance measurement which could only detect damage in a circuit of several solder balls. Since the dye only reaches cracked areas, partial damage to solder balls is easily identified by partial coloring.

3.7.2 Microsectioning analysis

Microsectioning analysis is a method to study cross sections of a PCBA optically. The sample preparation is a delicate process involving several critical preparation stages that require high precision tools. Since this kind of equipment was not available, microsectioning analysis was outsourced. The first step of the microsectioning analysis was to cut the PCBA specimens into smaller parts using a precision diamond saw. The specimens were then delicately placed in resin. After several steps of sanding and polishing of the resin enclosed specimens, they were inspected under a microscope to find possible cracks in the soldering.

3.8 Validation

In order to ensure that the method and model are applicable to PCBAs other than the specific cases it was calibrated for, validation was performed under new conditions. For this purpose, the same PCBA used for calibration but with new hole fastenings was used, as well a completely different PCBA.

3.8.1 Fatigue validation

In order to validate the model and method, three additional new hole fastenings were used. These were different from the four fastenings used for the calibration of the model, making sure that the model is not valid only for the specific calibration cases. The first fastening used was a combination of hole numbers 5 and 6, using all eight holes around the edge of the PCBA. The second was the same but using hole numbers 4 and 6. The final fastening used was all holes with number 5 and one hole with number 1. In a PCB design process this final fastening could be a feasible solution to stiffen the PCB around the BGA component. The three cases are visualised in figure 3.13, where the fastening points are marked with red circles.

All validation experiments and simulations were done using random vibration. Like for the initial random experiments, the PSD signal was converted to a $G_{3\sigma}$ value at the eigenfrequency of each specific fastening. The corresponding strain $E_{3\sigma}$ was computed using the method of two linear curves discussed in section 3.5, produced purely from simulations and application of the rule of thumb mentioned. These strain levels with corresponding measured number of cycles to failure were compared to the EN-curve for random vibrations, without further altering the linear fit.

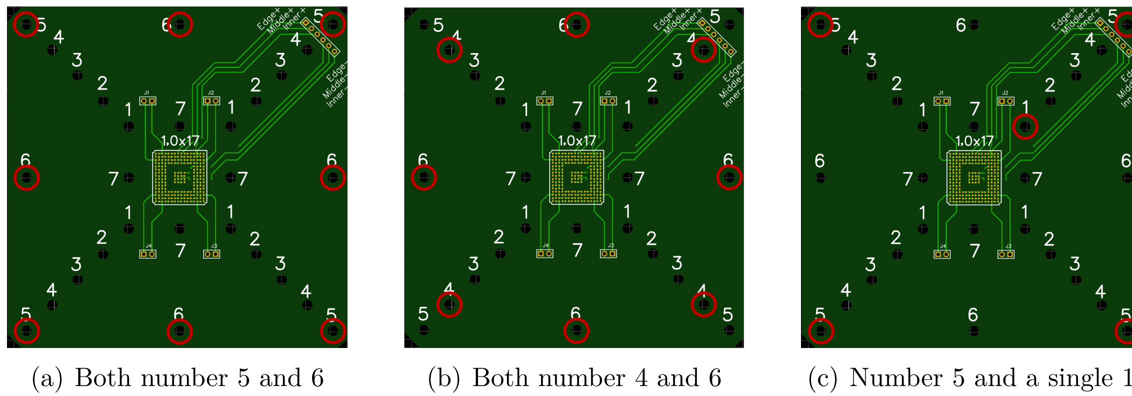

(a) Both number 5 and 6 (b) Both number 4 and 6 (c) Number 5 and a single 1

Figure 3.13: Description of hole fastenings used for the validation tests. The red circles marks the holes used for each case.

3.8.2 Strain validation of new unit

To further validate the developed method, a PCBA that was completely new to the project was investigated. This PCBA was designed by CPAC for assembling in one of the their products. It is a fully assembled PCBA with approximately 200 components and a thickness of 1.6 mm. Since the PCBA was not designed as a test board, continuous monitoring to detect failure was deemed impractical. Therefore the validation was performed only in terms of eigenfrequencies and strains. Figure 3.14 shows the PCB mounted with M3 spacers onto the fixture together with accelerometers and a strain gauge-rosette.

No calibration of any kind was performed. An existing CAD-model of the PCBA was used and modified into two different CAD-models. One model only including the PCB and one model including the full PCBA with both board and components. Both models were imported into Ansys. The material parameters and boundary conditions resulting form the calibration discussed in section 3.2 were used. The eigenfrequencies and strain levels obtained from the simulations were compared to corresponding experimental values, obtained in the same fashion as discussed in sections 3.4 and 3.5.

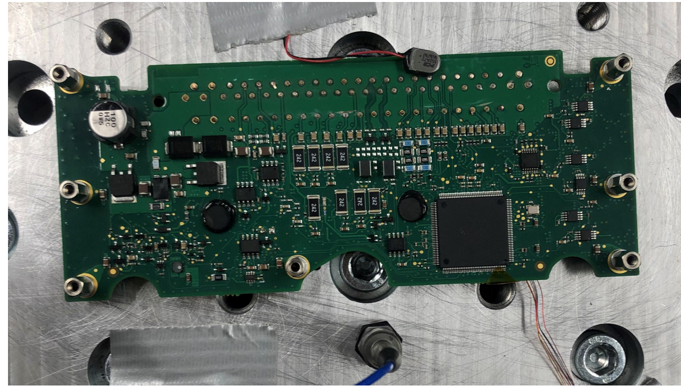

Figure 3.14: PCBA used for further validation, here mounted to the vibration fixture using M3-spacers.

4

Results

This chapter covers the results of the modelling of strain and acceleration compared with experimental measurements.

4.1 Calibration of material parameters

The sum of the diagonal terms in the MAC matrix are shown with corresponding values of E and m_{acc} in table 4.1. A sum of 5 would indicate perfect correlation for every mode, and a sum of 0 would indicate no correlation for any mode. As seen in this table the best results are found with lower values of m_{acc}, the very best being with $m_{acc} = 0.9\,\mathrm{g}$. Since the weight of an accelerometer without cable was measured to be 1 g, this is considered the minimum physically sound value. The weight of the cables do not seem to effect the vibrations of the PCBA. Increasing the value of E does improve the MAC values slightly, but much less than changing m_{acc}. The value of E is therefore considered as insignificant in terms of the MAC numbers, and is instead varied in order to fit the eigenfrequencies.

Table 4.1: Sum of diagonal elements in MAC matrix for different material parameters. BGA modelled with the same material parameters as the board.

E_{PCB} [GPa]	m_{acc} [g]	$\sum_{i=1}^{5} m(i,i)$
30.0	1	4.8318
27.0	1	4.8318
24.5	2	4.7799
24.5	1	4.8317
22.5	2	4.7791
22.5	1.5	4.8119
22.5	1.2	4.8260
22.5	1.1	4.8293
22.5	1	4.8316
22.5	0.9	4.8328
20.5	2	4.7787

The results of varying E in order to match eigenfrequencies is shown in figure 4.1(a). Regardless of whether the BGA component was included or not, the best match was found at $E = 19\,\mathrm{GPa}$. For the PCB with BGA mounted, this value assumes that the BGA is of the same material as the board. The fact that both versions have their best fit at $E = 19\,\mathrm{GPa}$ indicates that the contribution of the BGA is not significant

enough to change the global properties of the board. When modelling the BGA as a separate material, its value of E was varied to improve the fit to experiments, while the properties of the board were kept constant. The resulting error plot is shown in figure 4.1(b). As seen in this figure, the fit could then be improved further, with $E_{BGA} = 350\,\text{GPa}$ being optimal. The error does not vary much for values of E_{BGA} between 100-1000 GPa, indicating that this parameter does not have a large impact. The value 350 GPa is a very high stiffness considering that the BGA is composed of plastic, copper and solder material, none of which individually is likely to be so stiff. The value 350 GPa should therefore not be seen as the physical stiffness of the component in isolation, but rather its effective stiffness in the specific conditions on the PCBA. The value may include compensations for error in geometry or material models. All material parameters used in the model are listed in table 4.2.

Table 4.2: Calibrated or given material parameters. These numerical values are used throughout the rest of the report.

Property	**Value**	**Method**
E_{PCB}	19 GPa	Calibrated
ν_{PCB}	0.127	Given
ρ	1950 kg/m^3	Measured
E_{BGA}	350 GPa	Calibrated
ν_{BGA}	0.127	Given
m_{acc}	0.001 kg	Calibrated

A MAC plot for the final chosen parameters is shown in figure 4.2. The plot displays the desired characteristics of diagonal elements close to 1. The eigenfrequencies corresponding to the best fits of figure 4.1 are tabulated in table 4.3.

Table 4.3: Comparison of eigenfrequencies between simulation and experiment. The simulated eigenfrequencies are for the case of best fit for E_{PCB} and E_{BGA}. Columns $f_{sim,BGA}$ and $f_{sim,optiBGA}$ refer to simulations with $E_{BGA} = 19\,\text{GPa}$ and 350 GPa respectively.

Modes	$f_{exp,empty}$ [Hz]	$f_{sim,empty}$ [Hz]	$f_{exp,BGA}$[Hz]	$f_{sim,BGA}$ [Hz]	$f_{sim,optiBGA}$ [Hz]
1	199	230	199	240	247
2	397	365	401	371	376
3	426	374	442	394	405
4	548	566	548	566	567
5	560	576	562	577	579

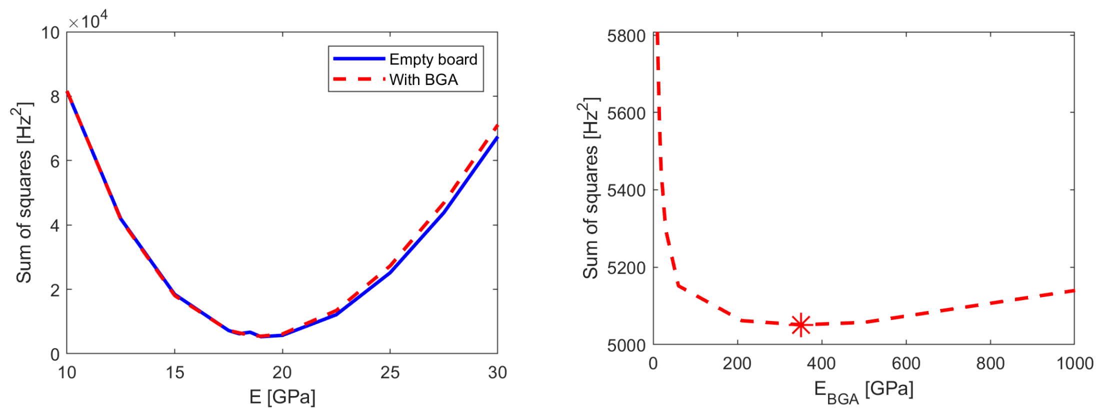

(a) The Young's modulus E is varied for the PCB with and without the BGA component mounted on it. The BGA is modelled with the same material parameters as the board.

(b) The Young's modulus E is varied for the BGA only, with $E_{PCB} = 19\,\text{GPa}$.

Figure 4.1: Sum of squares of difference between five first eigenfrequencies from experiments and simulations. Young's modulus varied for PCB and BGA separately.

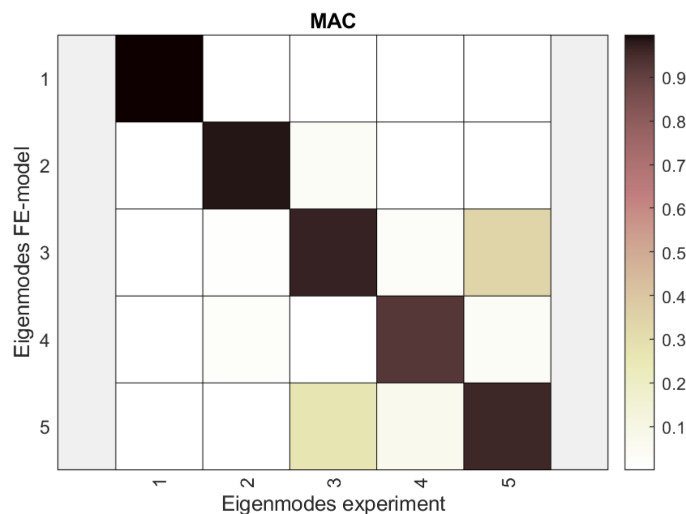

Figure 4.2: MAC-plot comparing the eigenmodes from test to simulation using the calibrated parameters of m_{acc}, E_{PCB} and E_{BGA}. The modes correlate well with a distinct diagonal and a MAC-value of 0.997 for the first mode.

4.2 Modelling of acceleration

In table 4.4, the frequency of greatest measured response acceleration in experiments is listed with corresponding eigenfrequencies from simulations. For holes 3-5, this is the first eigenfrequency, and for hole 6 it is the fourth eigenfrequency. Simulation numbers 1-4 refer to the method for modelling the fastening points, as discussed

in section 3.4 and should not be confused with hole fastenings. The RMS error is also listed, and is the measure used to determine which modelling method fits experiments the best. As seen in table 4.4, the most accurate results are obtained from simulation 4, with the smaller surfaces on top and bottom sides of the PCBA fixed. The method of only fixing an area on the top and bottom side of the PCBA is also the most physically sound. The inner diameter of the fastening holes on the PCB is not threaded, and allows some room for the screws to move. Thus, it is the screw and spacer clamping the board that fixes the PCBA in place.

Table 4.4: Frequency of maximum component acceleration for different hole fastenings and boundary conditions.

Hole	f_{exp} [Hz]	$f_{sim,1}$ [Hz]	$f_{sim,2}$ [Hz]	$f_{sim,3}$ [Hz]	$f_{sim,4}$ [Hz]
3	826	803	859	858	825
4	509	495	524	524	507
5	320	314	329	329	320
6	722	713	758	758	731
RMS [Hz]	-	14.5	26.0	25.5	4.94

The damping factor of the PCBA was calibrated by comparing the FRFs of experiment and simulation. The peak accelerations experienced by the component in experiments when using three different damping factors are shown in table 4.5. As indicated by the RMS value, 0.45 % damping is the best value out of the three. Since this is the middle value rather than one of the extremes the optimal value is assumed to be between 0.4 % and 0.5 %, and thus no further refinement was made.

Table 4.5: Maximum component acceleration [g] for different simulated damping factors and hole combinations with an input vibration of 0.1 g. RMS error compared to experiment.

Hole	Exp	0.4 %	0.45 %	0.5 %
3	13.8	16.1	14.3	12.8
4	17.3	17.8	15.9	14.3
5	13.3	17.3	15.4	13.8
6	16.4	18.9	16.9	14.9
RMS	-	2.63	1.30	1.81

In figure 4.3 the acceleration response from experimental data is plotted together with corresponding simulations. These simulations utilise the model version determined to be optimal, modelling the fastening points according to method 4 and using 0.45 % damping. The applied input acceleration was 0.1g. As previously shown in tables 4.4 and 4.5 the peaks of simulations and experiments match quite closely in both frequency and amplitude. Figure 4.3 shows that the response of simulations and experiments also match well for the rest of the spectrum. However, for hole profile 6, there is a local maximum at a lower frequency than the global maximum, which does not match very well between simulation and experiment. Hole profiles

4 and 5 also have a second peak slightly above 1000 Hz, where the simulations and experiments appear to diverge. Since the experiment was set to only sweep up to 1000 Hz, the specifics of the difference at these second peaks were not included in the study.

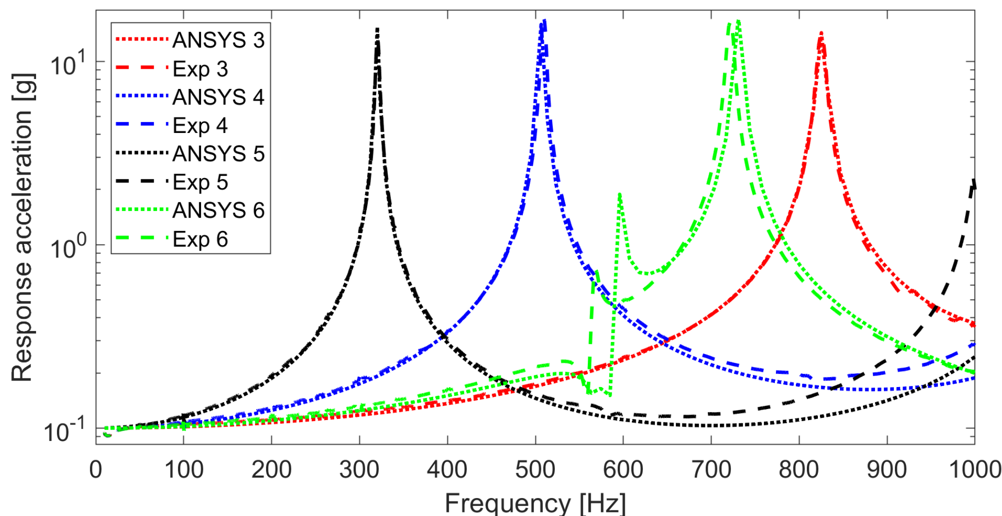

Figure 4.3: Experimental and simulated response accelerations at the BGA component for different hole fastenings. A constant input acceleration of 0.1 g was applied.

4.3 Modelling of strain

Both measurements and simulations have been performed as described in section 3.5. The results are visible in figures 4.4 - 4.7 for respective hole fastening. The strain of the PCBA underneath the component is plotted versus the acceleration of the fixture. For all four cases the simulated strain is proportional to the acceleration of the fixture in a fully linear manner. As can be seen from the experimental data points, red solid line, the strain is not behaving linearly with respect to the acceleration. The reason for this difference is that the simulation of the PCBA is not taking geometrical non-linearities into consideration, which is acceptable when small deformations are considered. In other words, for low acceleration levels of the fixture the PCBA are exposed for small deformations and the simulation should correlate with experiments. As seem from the results in figures 4.4 - 4.7, this is the case. The lowest experimental data points are located close to the simulated behaviour. When the acceleration increases, the deformations increase and the geometrical non-linearities and membrane effects start to play a greater and greater role, which results in slower strain increments.

The initial linear region is of varying accelerational interval depending on which hole fastening is used. In table 4.6 an approximate breaking point for when linearity ceases to apply is defined for each hole fastening. This breaking point varies between 0.9 and 3 g depending on the hole fastening. If the distance between the

holes increases, the transversal deformation also increases if the acceleration is fixed. This means that the linearity should cease to apply at lower accelerations for hole fastening 5 compared to hole fastening 3, as an example. This is confirmed by table 4.6. By computing the deformation angle, a rule of thumb can be formulated. This angle is stated in the bottom row of table 4.6 and varies between 0.2° and 0.28°. A rule of thumb can therefore be formulated for a PCBA of thickness 1.6 mm. This rule is that the strain behaves linearly with respect to the acceleration if the maximum deformed angle is less than approximately 0.25°.

Table 4.6: Different parameters at the breaking point from linearity for the different hole fastenings. Breaking point defined by visual inspection in the graphs.

	Hole 3	Hole 4	Hole 5	Hole 6
Acceleration [g]	3	1.5	0.9	3
PCBA strain [µm/m]	125	115	95	140
Transversal def [mm]	0.16	0.23	0.34	0.24
Deformation angle [°]	0.204	0.234	0.285	0.282

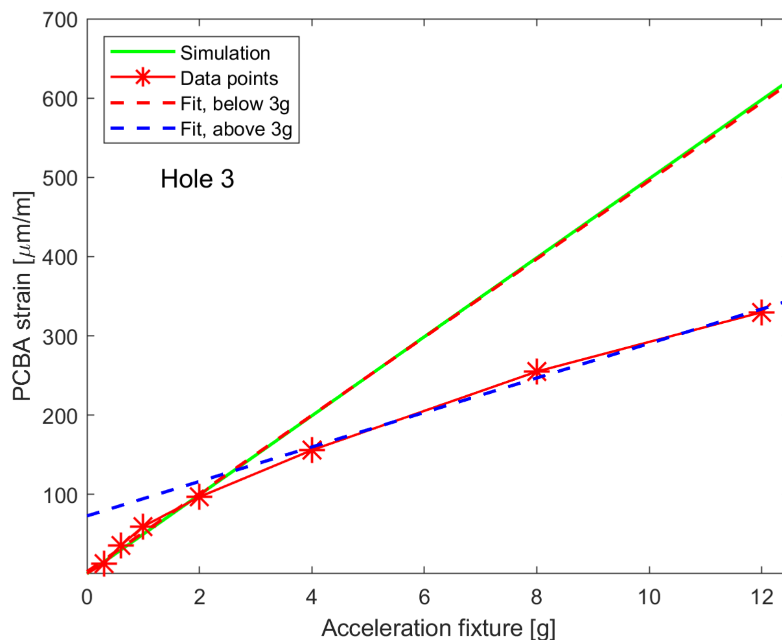

Figure 4.4: Simulated strain in green compared to experimentally measured strain in red for hole fastening 3.

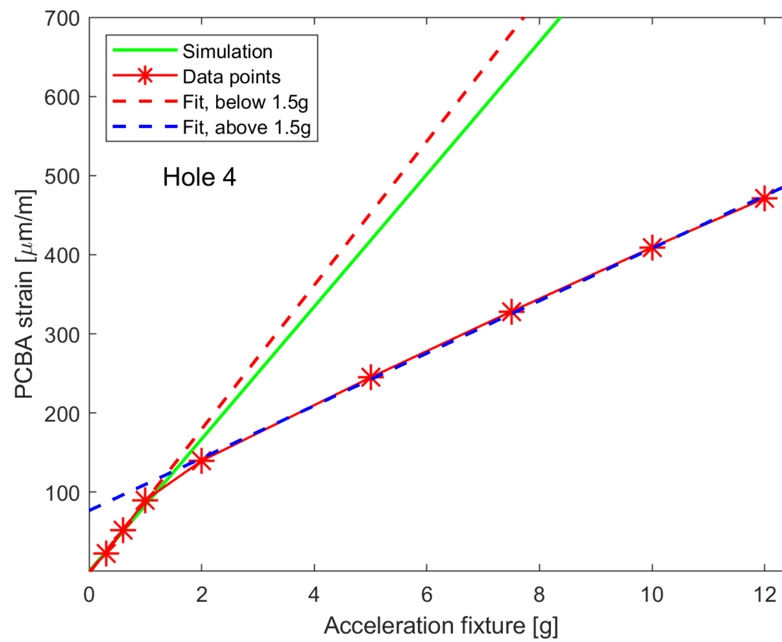

Figure 4.5: Simulated strain in green compared to experimentally measured strain in red for hole fastening 4.

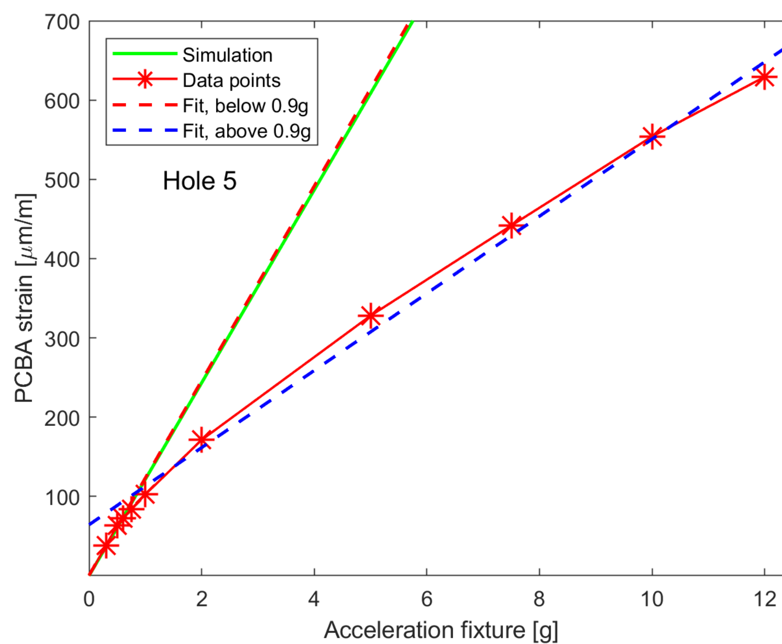

Figure 4.6: Simulated strain in green compared to experimentally measured strain in red for hole fastening 5.

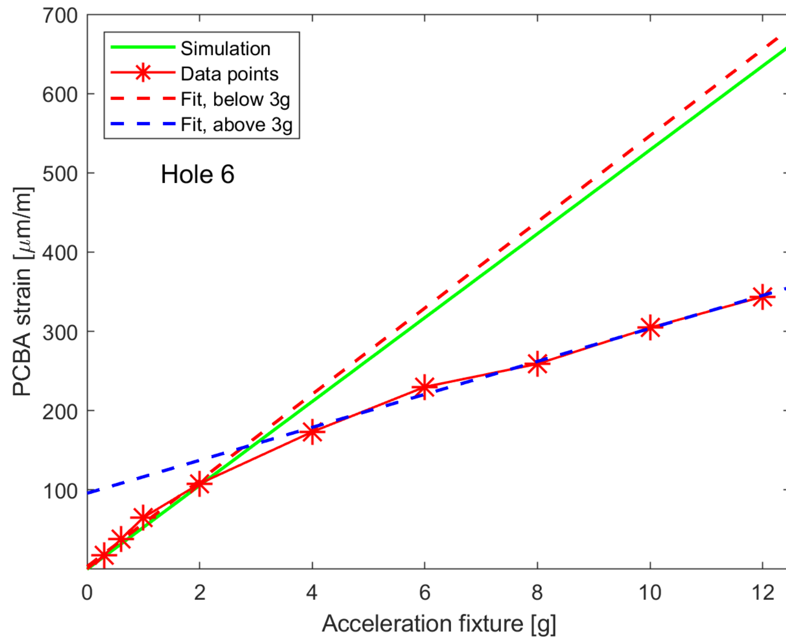

Figure 4.7: Simulated strain in green compared to experimentally measured strain in red for hole fastening 6.

For higher acceleration levels than the breaking point in table 4.6, the simulated strain can not be directly used. For each hole fastening in figures 4.4 to 4.7, a second linear fit is performed for the data points above the breaking point. The fits correlate rather well with the data points above the breaking point for all four cases. Notably, for all four cases the slope of the strain in the linear region is approximately 2.5 times larger than the slope in the non-linear region. More exactly, the factors are 2.30, 2.52, 2.50 and 2.54 in respective order for the four hole fastenings, with a mean of 2.47. This is the case at the eigenfrequencies, but outside of the eigenfrequencies both angle and slope will likely vary with frequency. This factor can be used as an correction to the simulation to be able to compute the correct strain even for an unknown new hole fastening. In figure 4.8, the final strain approximation is plotted together with its data points for the four hole fastenings. It consists of the initial fit below the breaking point and the second fit above the breaking points.

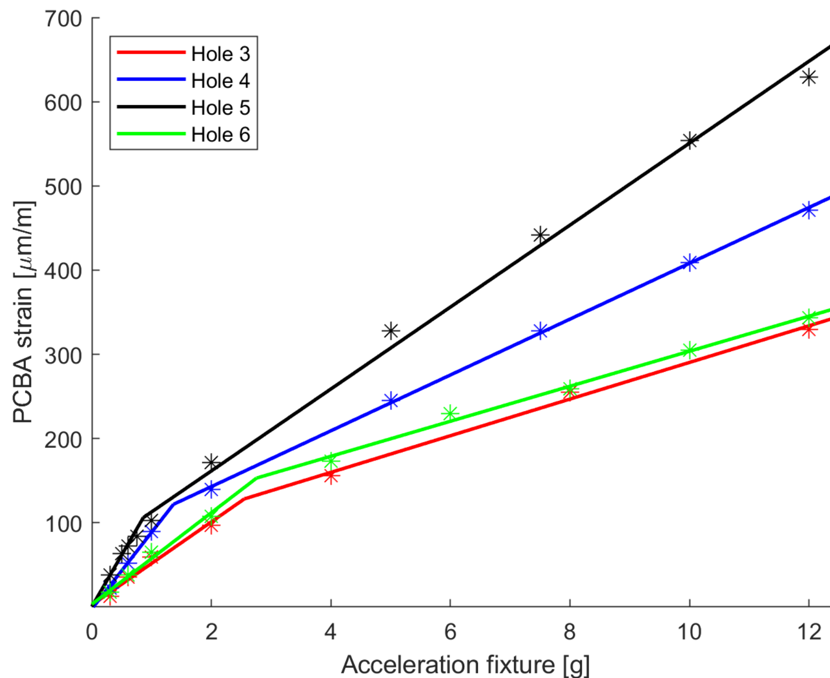

Figure 4.8: Linear approximations of measured PCBA strain as a function of input acceleration.

4.4 Harmonic vibration until failure

As described in section 3.6, experiments with harmonic vibration were performed to vibrate the PCBAs until failure occurred. The purpose was to produce an EN-curve for the PCBA to relate the number of cycles to failure to the PCBA-strain underneath the component.

4.4.1 EN-curve

The experiments at harmonic vibration were performed 40 times using a variety of input accelerations. The same four hole fastenings (3, 4, 5 and 6) as discussed in section 4.1 and 4.3 were used. The range of applied accelerational levels as well as total number of experiments for each hole configuration is shown in table 4.7. The frequency for each tested PCBA was chosen as the eigenfrequency giving the most severe strain under the BGA. Since the frequency was known, the number of cycles to failure could be determined by measuring the time to failure and multiply with the frequency. For a given input acceleration of the fixture is was possible to determine the PCBA strain by interpolation from the result of figure 4.8.

Table 4.7: A total of 40 experiments were performed distributed over the four hole combinations. A fixed acceleration from each respective interval was used during one complete run to failure.

Hole	Count	Input acc range [g]
3	8	8 - 10
4	12	5.5 - 9
5	12	4.5 - 9
6	8	7 - 11

The EN-curve for the simulated strain is given in figure 4.9. It consists of 40 data points plotted with cycles to failure on the horizontal axis and PCBA strain on the vertical axis. A linear fit (in log-scaled cycles) with least square is performed to the data points. Even though the spread of the data points is relatively large, the linear fit follows the desired behaviour, in that the PCBA can withstand more load cycles if the loading causes low PCBA strain-levels compared to high strain-levels. The equation for the fit can be written as

$$\epsilon = -53.9 \log_{10} N + 622 \tag{4.1}$$

with N being the number of cycles and ϵ being the strain in µm/m. The data points have a mean deviation in strain from the linear fit of 11.3 %, which is stated and compared to other results in table 4.8. A spread in the data points is expected since there is a stochastic element to fatigue. It is also worth noting that the number of cycles to failure are in the region of 10^4 and 10^7, which is the region for high-cycle fatigue.

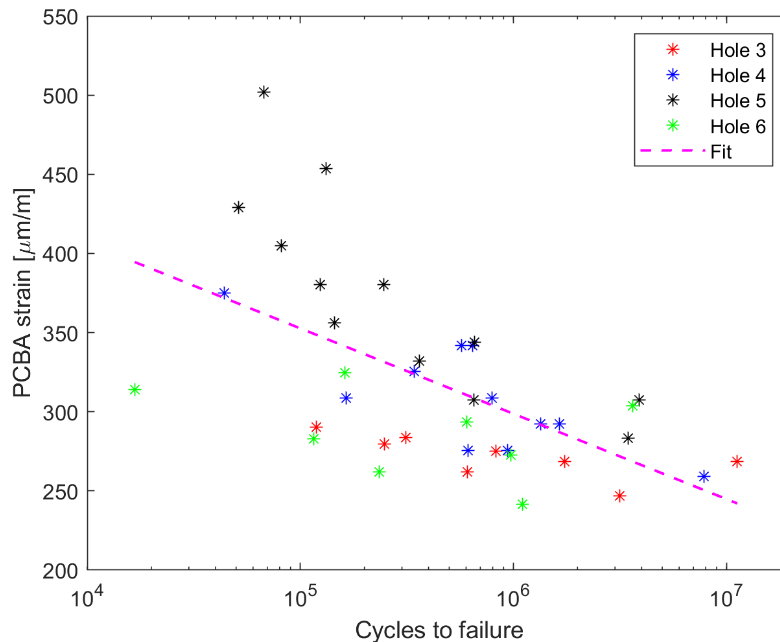

Figure 4.9: EN-curve relating cycles to failure to strain levels of the PCBA. A linear fit is performed to the data points showing a trend of increasing cycles to failure for lower strain-levels. Different colors indicate different hole fastenings.

In figure 4.9 all 40 points from all four variations of hole fastenings are plotted and analysed together. However, as seen in this figure, the different hole fastenings do not behave in quite the same way. Most notably, the data points for hole 5 are all located at or above the linear fit. This effect is especially prominent for the shorter lifetimes, below $3 \cdot 10^5$ cycles. In contrast, a majority of the points for holes 3 and 6 are located below the line, and the points for hole 4 spread around the line. With this in mind, it is of interest to analyze the hole fastenings separately, or with some holes excluded, to improve the linear fit. This is done in figure 4.10, where the different sub figures have data points filtered based on different hole fastenings. The corresponding mean deviation of the data points in each case are given in table 4.8. Hole 3 has the lowest mean deviation in strain at 2.6 %, while holes 5 and 6 have the highest deviation, both at 7.3 %. Any hole fastening on its own shows a lower deviation than the combined case, which is expected. However, the combined case is more desirable since the resulting EN-curve should be applicable for different PCB-designs and hole fastenings. Excluding only hole 5, as done in sub-figure (e) of 4.10, gives a mean deviation of 7.5 %, only slightly higher than using hole 6 on its own. Based on this, it could be argued that hole 5 should be excluded from the analysis. It is still included in all results going forward, in order to give the most general result possible.

Table 4.8: Relative mean absolute error values for different hole fastenings.

Hole	$MAER$ [%]
All	11.3
3	2.66
4	5.20
5	7.26
6	7.26
4,5	8.10
3,4,6	7.53

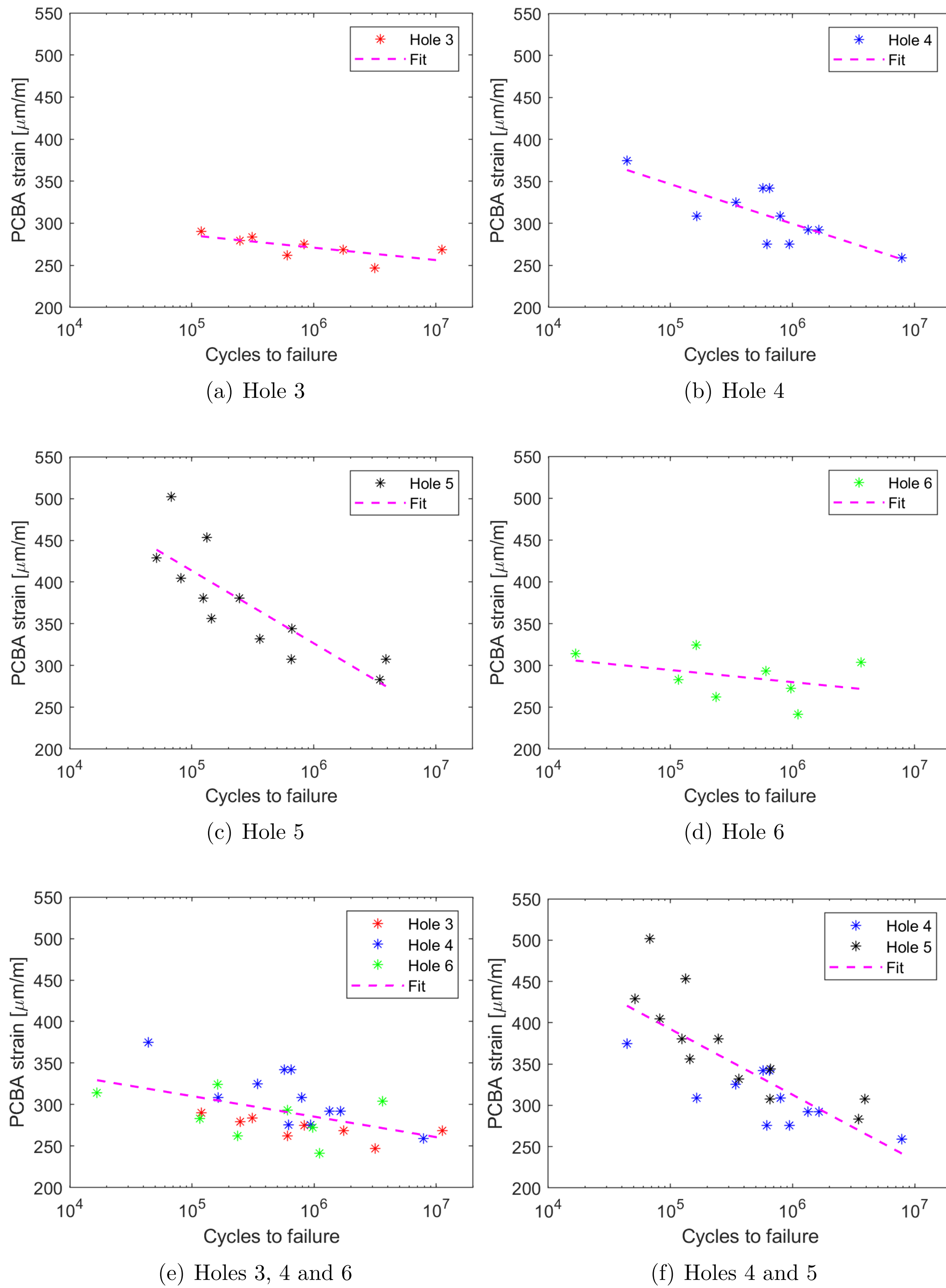

(a) Hole 3 (b) Hole 4

(c) Hole 5 (d) Hole 6

(e) Holes 3, 4 and 6 (f) Holes 4 and 5

Figure 4.10: EN-curves with filtered data points based on hole fastening.

4.4.2 Statistical analysis

The same least squares fit as in figure 4.9 is shown again in figure 4.11, together with a Theil-Sen fit. As can be seen in this figure, the two regression models produce similar results for the data. As discussed in section 2.6.1 the least square method is more sensitive to outliers than Theil-Sen. Therefore the close match between the two fits indicates that outliers do not have a great effect on the least square result.

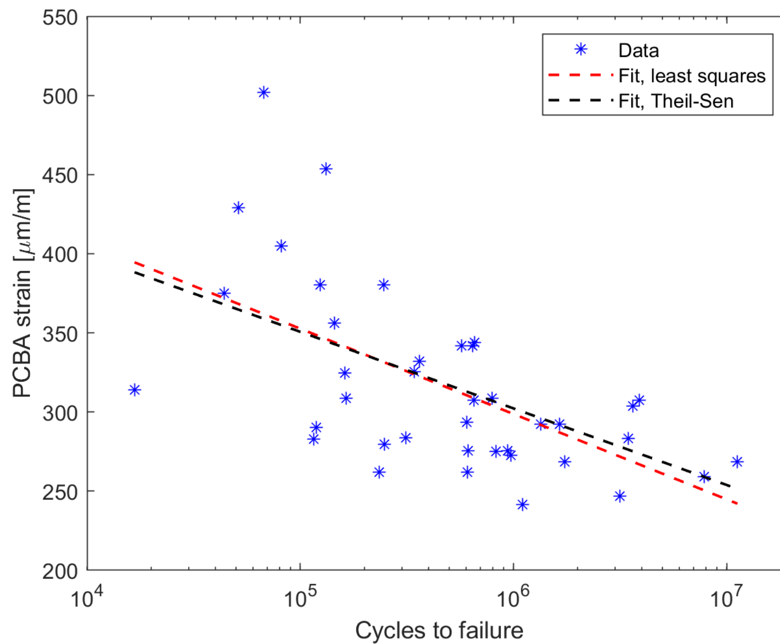

Figure 4.11: Least square fit of simulated strain levels together with Theil-Sen fit.

The linear fits of 20 bootstrap sets are shown in figure 4.12, together with the linear fit of the original data set. The bootstrap plots are quite close to the original fit in the range of $5 \cdot 10^5$ to $1 \cdot 10^6$ cycles. This is because this range contains the largest number of data points, meaning that the bootstrap sets will typically have to conform to fit well in this range. It can be noted that the slopes differ more on the negative side of the original fit than they do on the positive side. This skewness is caused by a number of points that for short lives have a larger strain than expected for the measured life. When these points are sampled often, and combined with certain other data points, the resulting slope is steep. Since there are essentially no corresponding points that have a lower strain than expected for the short lives, there will be few sets of points that can cause slopes that differ to the right.

The relatively small number of bootstrap sets generated for figure 4.12 was chosen to make the plot clear. If more lines were produced, extremes in terms of slope and intercept would be more likely to be generated.

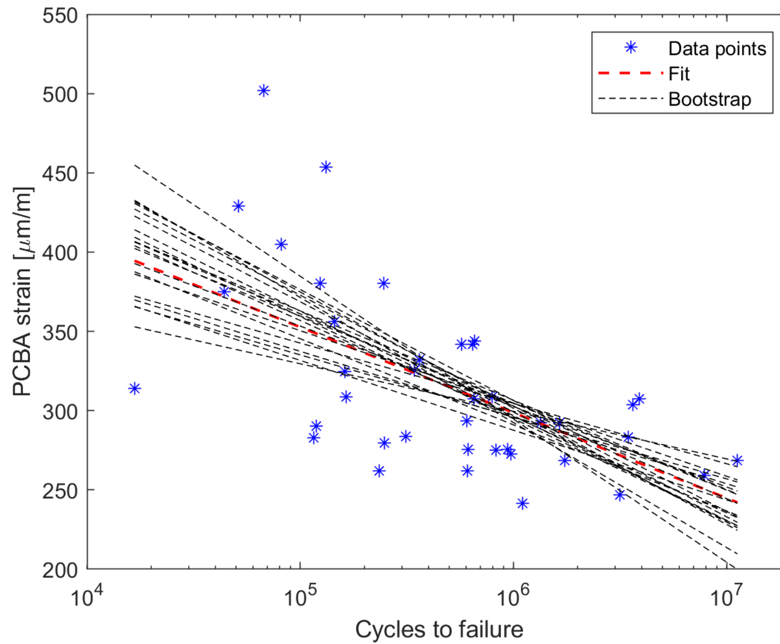

Figure 4.12: Least square fit of original data set and 20 bootstrap sets.

The distribution of slope values from 1000 bootstrap sets can be seen in figure 4.13. As seen in this figure, the distribution is nearly normal, but is skewed to the left, meaning that the values below the peak of the distribution are more likely to occur than they would be for a normal distribution. The histogram confirms the spread in the results. The standard deviation of the bootstrap slopes is $\sigma = 14.9$ and the mean $\mu = -55.2$. This means that 68 % of values will be in the range of -40 to -70. This is likely to be the range of slopes if the experiments would be reproduced.

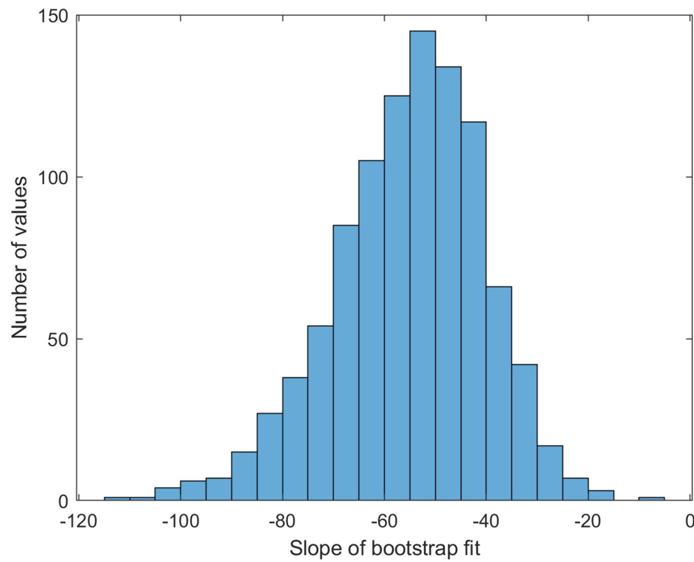

Figure 4.13: Histogram of slope values computed from 1000 bootstrap sets. Least square fit. $\sigma = 14.9$, $\mu = -55.2$

The linear fit is plotted together with one standard deviation in figure 4.14. As an example, if a PCBA is specified to withstand one million equivalent cycles, the allowable strain underneath the corner BGA soldering is between 251 and 347 µm/m if an uncertainty of one standard deviation is considered.

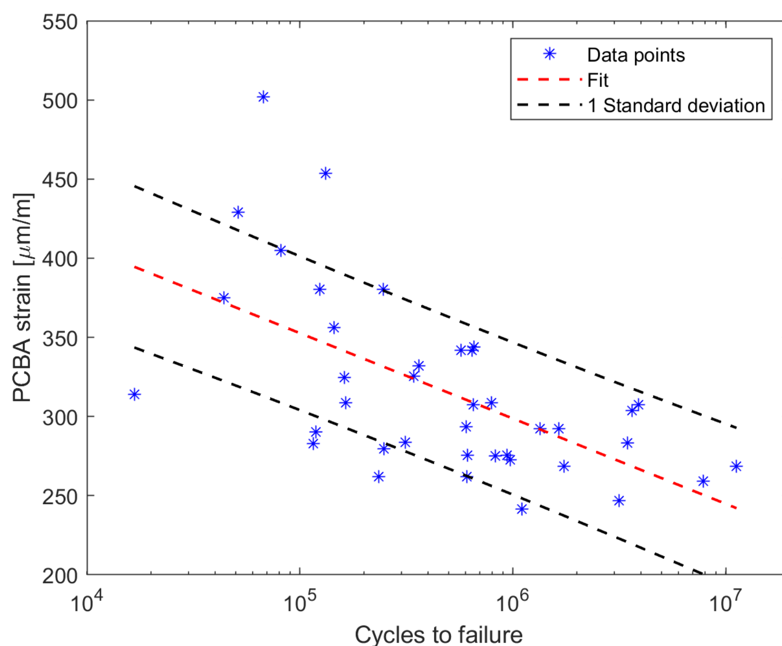

Figure 4.14: One standard deviation with respect to the harmonic data points are given by the black dashed line.

4.5 Random vibration until failure

The same type of experiment as for the harmonic case was also performed for the case of random vibration.

4.5.1 EN-curve

In figure 4.15 an EN-curve for PCBAs subjected to random vibrations is shown. Note that the strain is the computed 3σ-strain based on Miles' equation for each accelerational level and hole fastening, see section 3.6.2. The number of cycles is an equivalent measure, obtained by multiplying the time to failure by the most severe eigenfrequency of the PCBA. With equivalent number of cycles on the x-axis, the data points have a mean deviation in strain of 9.55 % from the linear fit. The expression for the linear fit is given as

$$\epsilon = -\log_{10}(N)\,35.7 + 398, \tag{4.2}$$

with board strain ϵ in µm/m and equivalent number of cycles N. The linear fit follows the expected trend and the computed strain 3σ values seems to be a reasonable measure of the severity of the vibration. Studying the different hole fastenings, hole 3 and hole 6 is closest to the fit while some data points of hole 4 and 5 deviate. The spread of the data points is of the same magnitude as for the harmonic case.

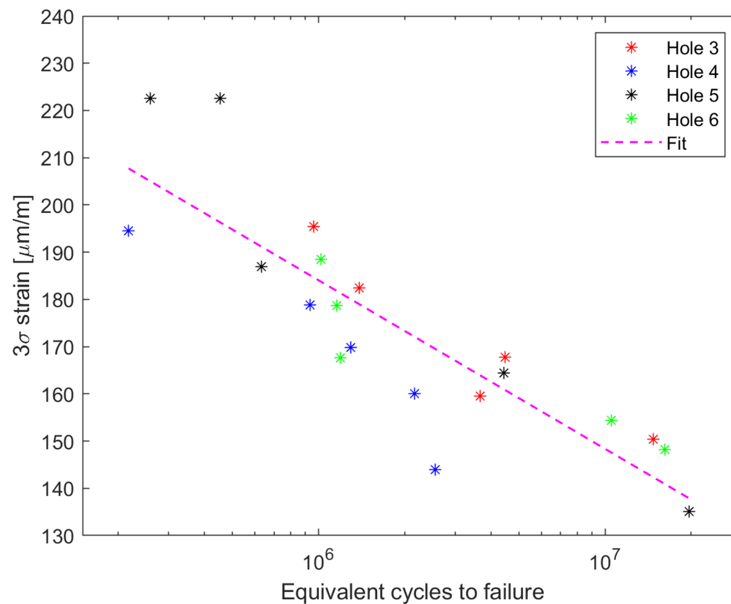

Figure 4.15: Measured lifetime in equivalent cycles for random vibration with 3σ strain from Miles' equation on the y-axis. Average relative error is 9.55 % .

4.5.2 Fatigue in middle circuit

Fatigue failure was also examined in the middle circuit, but only for 8 out of the 20 random vibration experiments. For each hole fastening, the two experiments with the highest computed 3σ strains were chosen as candidates for the middle examination. For these experiments, the same vibration continued until failure had occurred for both the outer and the middle circuit. The time to failure in the middle circuit was measured and converted into equivalent cycles by multiplying with the eigenfrequency. The results of the eight middle circuits are plotted in figure 4.16, where the colours represent different hole fastenings. The mean deviation of the middle failures is 6.18 %. The failures in the outer circuits are included as well for reference. For all eight experiments, the middle circuit withstood more cycles than the outer circuit. The two linear fits are nearly parallel, with slopes of $k_{out} = -35.7$ and $k_{mid} = -35.3$. At the average strain-level of 173 µm/m, the middle circuit withstands 8.2 times more equivalent cycles than the outer circuit computed based on the linear fits. If the two lines were entirely parallel, there would be a constant factor between the number of cycles to failure for the outer and inner circuits.

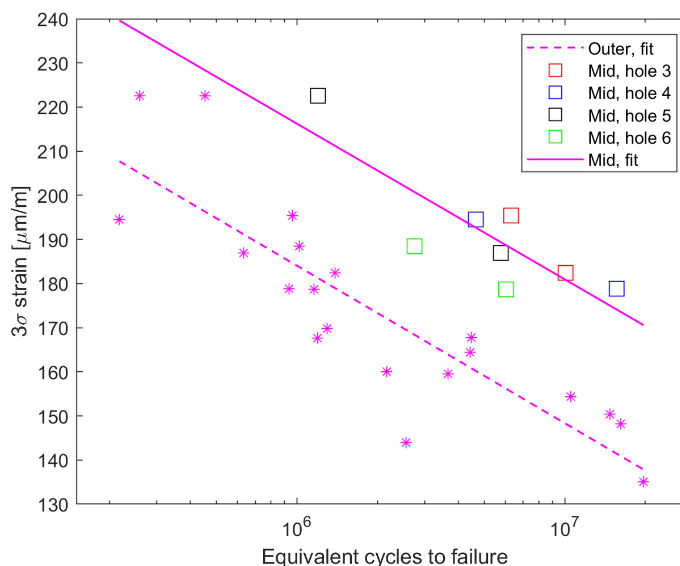

Figure 4.16: Lifetime of outer and middle circuit in equivalent cycles for random vibration. The middle circuit can withstand 8.2 times more cycles at the same strain level compared to the outer circuit.

4.6 Validation

Two types of validation were performed, using the same PCBA with new hole fastenings and using a completely new PCBA.

4.6.1 Fatigue validation

The results from the validation of PCBAs with new hole fastenings, discussed in section 3.8.1, is shown in figure 4.17. The six validation points are plotted together with the original data from figure 4.15. As seen in this figure the two data points from hole fastening 56 match the expected values reasonably well. They fit the line roughly as well as the original data. On the other hand, hole fastening 51 does not give results that match the fit at all. The mean deviation is 26.8 % for all six validation points and the error decreases to 8.65 % if hole fastening 51 is removed.

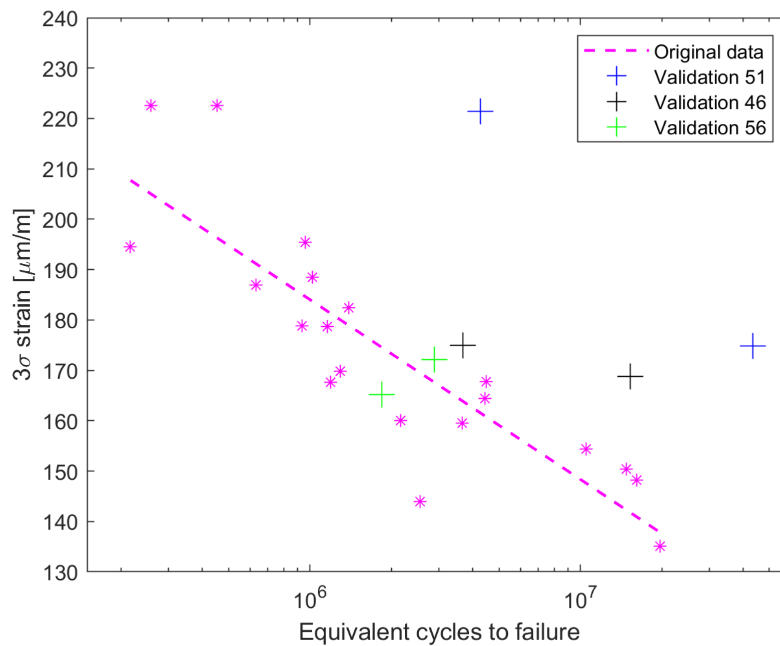

Figure 4.17: Six validation points, plotted together with original data points and its linear fit.

To give insight to why hole fastening 51 did not match the other results, strain measurements were performed at the corner that suffered the highest expected strain. In figure 4.18 the simulated strain for hole fastening 51 is plotted versus the input acceleration. The red dashed line is the approximated strain based on the rule of thumb regarding 0.25° angle deformation and the strain correction factor of 2.5, see section 4.3. This is the approximated strain behaviour used for the validation in figure 4.17. The experimentally measured strain is also plotted in figure 4.18. They match the approximated strain very well and mitigates doubts about the strain approximation not being valid for hole fastening 51. It also confirms the discussed rule of thumb for how to handle non-linearity.

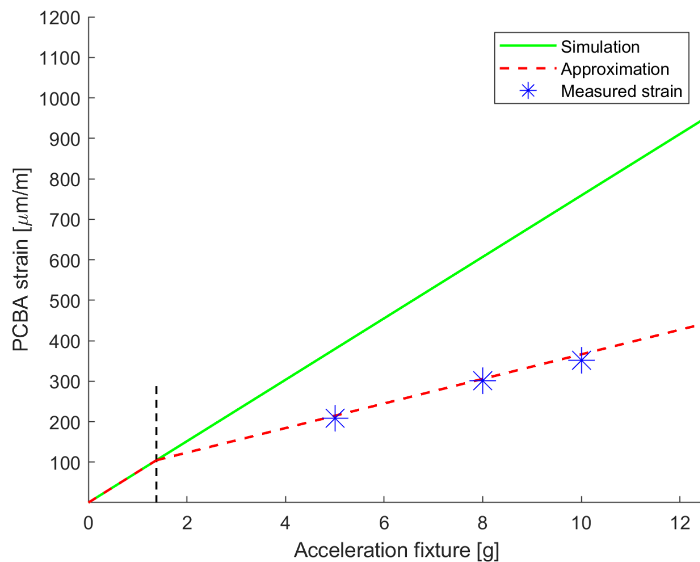

Figure 4.18: Validation of strain approximation for Hole 51. No fit is performed to the measured strain, the approximation (red) is only based on simulated strain.

4.6.2 Strain validation of new unit

The validation PCBA has three eigenmodes below 1000 Hz, with eigenfrequencies stated in table 4.9. As can be seen from the table, the model with the empty PCB correlates best to the experiments in terms of eigenfrequencies. The components were assigned the same stiff FR4 material as the PCB, which can explain why the eigenfrequencies are higher for the assembled model.

Table 4.9: Comparison of eigenfrequencies between experiment and simulation for validation PCBA. Simulations performed with and without components.

Modes	f_{exp}	$f_{sim,empty}$	$f_{sim,comp}$
1	300	296	309
2	576	595	589
3	750	780	794

Since the validation PCBA did not have any BGA components to check for failure, it was not possible to validate the EN-curve further. However, the strain approximation could be validated. Figure 4.19 shows the simulated strain as a function of input acceleration. The red dashed line is the approximated strain computed from the simulated strain according to the rule of thumb. The dashed black line marks when the PCBA has deformed 0.25°, which occurs at 0.65g. When considering the measured strain the linear region appears to be valid for higher accelerational levels than 0.65g. This also explains why the strain approximation is too low for the interval of 1 to 6g. The average relative error is computed to 14.2 % between the measured data points and the approximation. For the initial linear region the measured and simulated strain correlate very well.

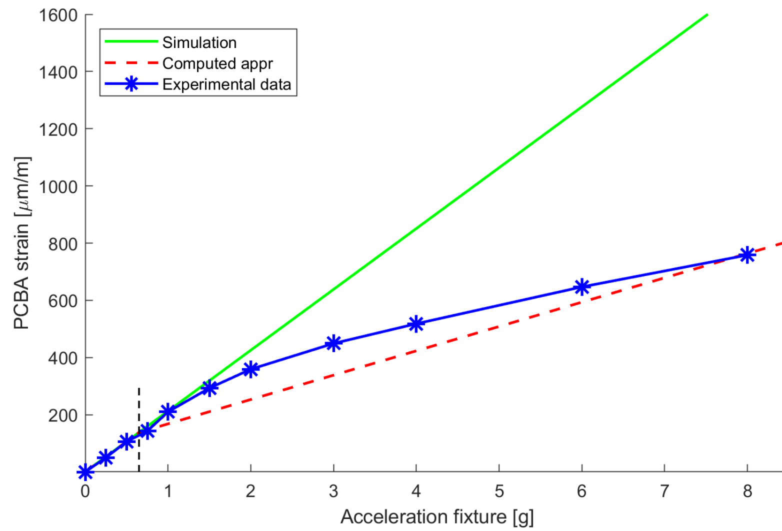

Figure 4.19: Comparison between computed and measured strain as a function of input acceleration. Break point at 0.65g to obtain deformed angle of 0.25°.

The result in figure 4.19 indicates that the rule of thumb is not perfect. Another rule of thumb found in literature suggest that if the deflection of the plate exceeds half of its thickness, then non-linear effects are significant [16]. This alternative rule of thumb was found not to be valid for the PCBAs mainly used in this study but for the validation PCBA the alternative rule using deflection and thickness appears to work well. In figure 4.20, the breaking point for linearity is defined based on when the PCBA has deformed 0.8 mm, half of its thickness. For this case, the strain approximation corresponds better to the test data than was seen in figure 4.19.

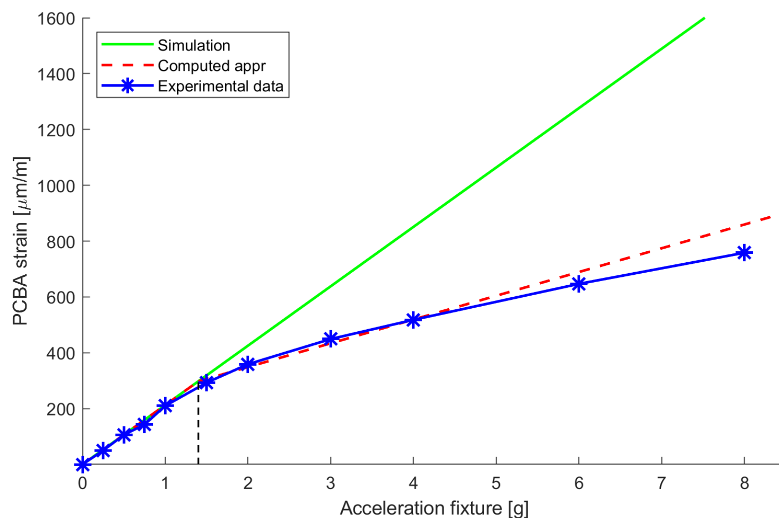

Figure 4.20: Break point at 1.4g to obtain 0.8 mm deformation (half thickness) at worst position.

4.7 Failure modes

The two methods for analysing failure modes have different uses and requirements. Both results show damage to solders with heightened resistance.

4.7.1 Dye-and-pry analysis

Figure 4.21 shows the results from the dye-and-pry process of a PCBA. The solderings in all four corners were damaged, but only in the outer circuit. No damage was visible on the middle and interior solderings. The figure shows a selection of some of the damaged solderings. In 4.21(a) two solderings that are red over the whole soldering area are shown. This likely means that cracks have penetrated these solderings completely which has enabled the red dye to colour the entire surface. On the other hand, figures 4.21(b) and 4.21(c) show solderings where cracks have started to propagate into the soldering but not all the way through. This is visible since the dye only covers a fraction of the soldering surface. The damage visible from the dye-and-pry analysis is consistent with the resistance measured manually before the dying process. The corner corresponding to figure 4.21(a) showed a much larger resistance than the other three corners. The resistance of the two inner circuits was also low.

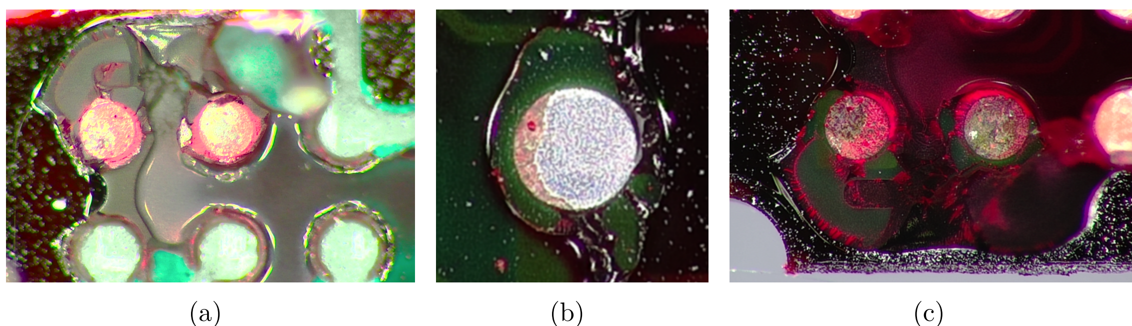

(a) (b) (c)

Figure 4.21: Results from DnP analysis. Red parts on solderings indicate damage.

4.7.2 Microsectioning analysis

Results from microsectioned BGAs inspected in an optical microscope are shown in figure 4.22. Both PCBAs were subjected to the same level of harmonic vibrations, but failed after a different number of cycles. $PCBA_{165}$, with the soldering shown in figure 4.22(a) failed after 165 000 cycles, while $PCBA_{792}$ in 4.22(b) failed after 792 000 cycles. $PCBA_{165}$ has a large void with a diameter of roughly 50 µm, through which the crack runs. $PCBA_{792}$ also has a void along the length of the crack, but it is significantly smaller. Voids can cause stress concentrations due to the geometry and also reduce the amount of material available to carry the applied load. Thus it is possible that the presence of voids reduces the fatigue life of a specimen, which seems to be the case when studying the results in figure 4.22.

The cracks in figure 4.22 run along the top side of the solderings, the BGA side. This is the thinnest part of the solderings. The difference in thickness between the two sides is due to the BGA side being solder mask defined, and the PCB side non-solder mask defined. This is a choice made in the design process of BGAs and PCBAs, and has implications for the manufacturing process.

When probing failed PCBAs, some corners displayed a heightened resistance compared to a new PCBA. When cross-sectioned, these corners also showed visible cracks, while the corners with a low resistance did not. This indicates that the raised resistance is actually due to damage in the solderings, thus confirming resistance measurements as a suitable method for detecting mechanical damage.

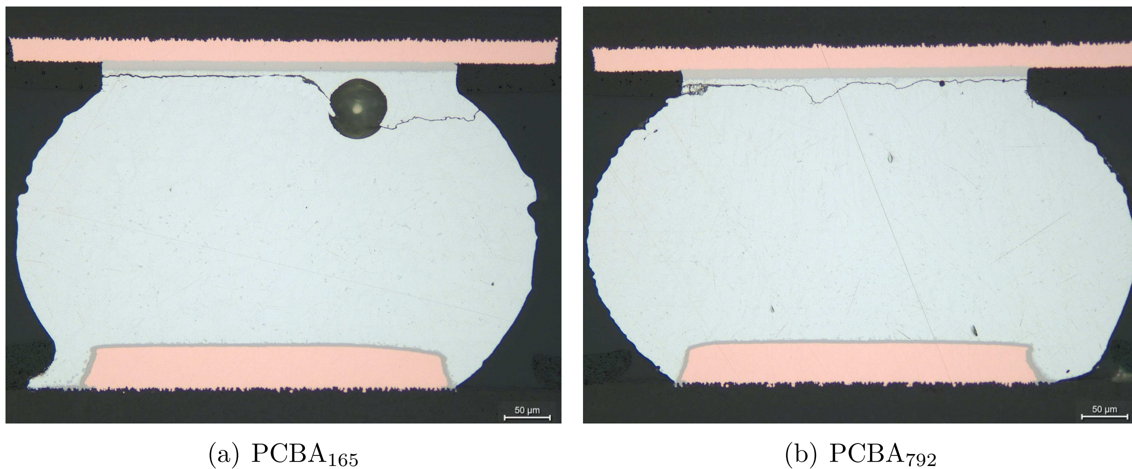

(a) $PCBA_{165}$ (b) $PCBA_{792}$

Figure 4.22: Cross section of solderings from two PCBAs inspected in optical microscope. Magnified 200 times.

Another possible reason for the spread is a difference in orientation of the crystalline structure of the solder. Figure 4.23 shows one entire row of solderings from $PCBA_{165}$ and $PCBA_{792}$. The respective row includes the soldering where the critical failure occurred. These images were taken using polarised light, which allows differentiation of the different crystal orientations. The different orientations are indicated by the colour difference of the solders. Since these orientations can not be controlled during the soldering process, they will be random for each solder ball. Due to the anisotropy of the crystal, the orientation makes a difference in terms of mechanical properties, thereby potentially affecting the fatigue life. For example, if a corner soldering is oriented so that it is especially stiff in the load direction, it will experience higher stresses for a given strain. Furthermore, some solderings have several different orientations present. The boundary between such areas are more susceptible to damage.

The shape of the solderings can also be noted in figure 4.23. The corner solderings are flattened, compared to the rounder solderings in the middle. This distortion is not symmetrical about the middle of the BGA and is not identical between specimens.

The variation in shape is caused by the difference in thermal expansion coefficients of the different materials in the PCBA and is indicative of residual stresses in the solderings. Therefore, it can also affect the fatigue life.

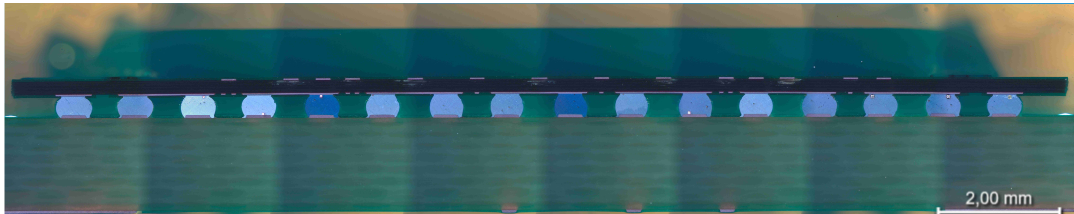

(a) PCBA_{165}

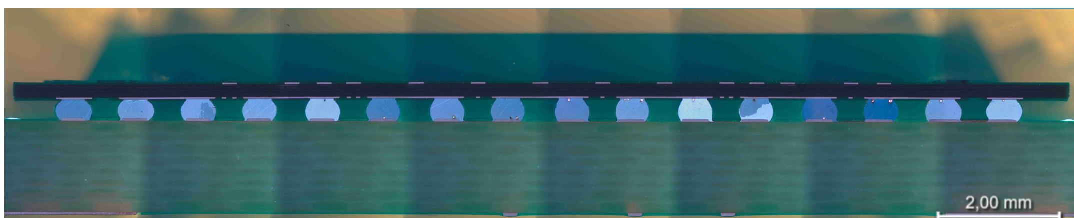

(b) PCBA_{792}

Figure 4.23: The row of solderings from the two different PCBAs where the critical failures occurred. Images are stitched using several different photos, all taken using polarised light.

5
Conclusion

In conclusion, it is possible to approximately predict the lifetime of a BGA-component due to mechanical fatigue. However, the large spread in experimental data results in relatively high uncertainties. This spread in lifetime is an important result in itself. There are many parameters that affect the lifetimes of test specimens, both testing conditions and variation during production.

5.1 Experimental setup

Overall the experimental setup worked well. The shaker, PCBAs, strain gauges and resistance measurements all performed as desired. However, some aspects of the experimental setup could be improved. For example, the accelerometer measuring the component acceleration should perhaps have been replaced. Before each harmonic experiment, a quick harmonic sweep was performed to find the individual primary eigenfrequency of each PCBA. This was measured using the accelerometer placed in the middle of the PCBA. It was noted that the accelerometer became more and more unstable as the experiments went on. In figure 5.1, the measured eigenfrequency for each PCBA is plotted together with the experiment number. As can be seen from the figure, the eigenfrequencies in general shift a little to the left (lower frequencies) for increasing experiment number. The effect is not significant however, and should not play a major role for the results.

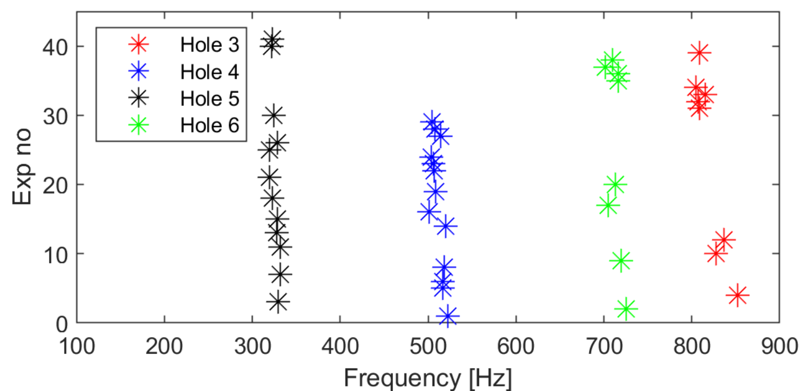

Figure 5.1: Measured primary eigenfrequency plotted for each harmonic experiment. Higher experiment number indicates that the experiment was performed later in the project.

As well as this shifting down, the eigenfrequencies also varied between two consecutive runs. This variation is undesired and is likely caused by imperfections in the experimental setup. The most likely cause is a difference in how tightly the PCBA was clamped between screw and spacer. There may also have been variations in PCB manufacturing or the soldering process. When computing the cycles to failure for the EN-curve the specific measured eigenfrequency was multiplied with the time to failure. The effect of varying eigenfrequencies should therefore not give the wrong number of cycles.

The strain measurements were an important part of the project in order to correlate accelerational level to PCBA strain. These measurements are the foundation for the EN-curve. Therefore it would have been desired to perform the strain measurement on more than one PCBA. Several measurements were performed, but they all used the same strain gauge glued to one PCBA. Variations in the PCBA manufacturing or the soldering are therefore not reflected in the strain measurements. The optimal procedure would have been to measure the strain on every experimental run to get a very exact EN-curve. However, this would also have been expensive and time consuming since once a strain gauge is fixed, it can not be reused on another PCBA. It was therefore a very positive result that the computed strain (based on simulation) for the validation hole-fastening correlated so well with experiments, as can be seen in figure 4.18. It confirms that the tuning of the FE-model performed well.

5.1.1 Resistance measurements

Figure 5.2 shows an example of how the resistance varied with time in the outer circuit during one of the experiments. At first the resistance is 82 Ω as it should, and after approximately 950 s the resistance starts to increase. This is indicative of a crack starting to propagate through one or more solderings. The resistance increases further until it suddenly rises to far above 190 Ω at 1136 s. This sudden spike is interpreted as a complete break of the soldering. Failure is considered to occur when the resistance is doubled from the original 82 Ω. When failure occurs, it is normally a high and clear peak, as seen in figure 5.2. The definition for the resistance threshold level is therefore not very crucial for the result.

If the experiment was not paused after a break, the resistance would typically not stay at the highest levels, but instead vary greatly between this total break and values well below the break limit. This is thought to be caused by the two faces of the broken soldering alternating between being separated and in contact due to vibrations.

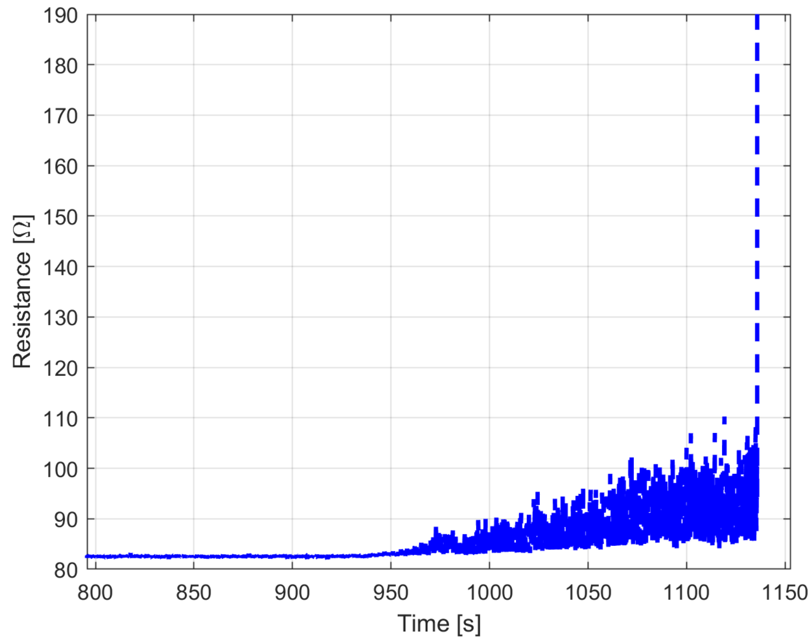

Figure 5.2: Example of resistance measured as a function of time during harmonic vibration.

While the resistance plot shown in figure 5.2 is quite typical for the data set, not all PCBAs showed this same behaviour. Some experiments displayed a much more sudden break, with very little propagation time. The reason behind this may be that damage only occurs in one single soldering, and that the resulting increase in resistance is very small until complete fracture occurs. The more typical plot might be a result of several solderings all sustaining some damage before one finally breaks.

There were also instances of the resistance not suddenly spiking, but instead climbing in a more continuous manner until reaching the threshold value of 164 Ω. In these cases it may be that several solderings experienced damage, and the combined increase in resistance from many smaller cracks was enough to raise the resistance above the threshold. These data points are also problematic because the threshold value is somewhat arbitrary. When the resistance climbs without spiking, the threshold value can make a difference in the number of cycles to failure. With a spike, the peak level is most often high enough to register as a break regardless of the level chosen. In conclusion, there appears to be several failure modes and damage mechanism at play in the results. Investigating these effects is some important future work in order to fully understand the mechanism behind the failures.

Furthermore, after the vibrations were stopped the resistance would typically stabilise around a value only slightly above 82 Ω. This may be caused by an effect known as crack closure, where the two faces of a crack may remain in contact even as an applied load is acting to separate them. It is also possible that the two halves are simply resting against each other, or held together by residual stresses in the PCBA. A real component might function well under such circumstances, since it

would still be connected as desired, only with a slight increase in resistance. This effect may cause problems when analyzing failed electronics, since the test environment is likely free from severe vibrations, unless deliberately added. On the other hand, performing the analysis in an environment with vibrations present may pose practical challenges, and if the vibrations are too severe further damage may be caused to the components.

5.2 Spread in results

As discussed in section 4.4.1 the spread in the results are quite large, making predictions difficult. This demonstrates the value of testing several specimens of the same product. It also justifies environmental testing with harsher conditions than expected in the life cycle. If the tested specimens happen to be unusually resilient and pass a harsh test, it indicates that more typical specimens will be able to sustain the expected vibrations. This is especially true since PCBAs with a purpose beyond testing are likely to be more complex, and also mounted in a casing with additional properties that may vary from case to case. The spread in results in this study is larger than some other works [8].

One reason behind the spread in the results is likely the existence of imperfections in the solderings. In section 4.7.2, the microsectioning analysis shows cross sections of two PCBAs subjected to the same level of vibration but with very different number of cycles to failure. Here, the existence of voids is believed to be one explanation. The PCBA with fewer cycles to failure has a very large void in the corner soldering where failure occurred. The other PCBA, which withstood almost five times as many cycles, has a very small void where failure occurred. In both cases, the crack intercepts the void. Apart from voids, residual stresses and orientation of crystals may play a part. This sensitivity to imperfections in the solderings applies for every performed experiment and gives a likely explanation of the spread in the EN-curves. The imperfections are inevitable and their randomness makes it difficult to estimate the lifetime with accuracy. The sensitivity highlights the importance of a high quality soldering process, to limit the number of voids as far as possible.

Another possible cause for the spread is a difference between hole fastenings, see figure 4.10. As discussed, hole 5 in particular displays a different behaviour than the others. Specifically, the strains of hole 5 are quite high, with the six highest strains occurring at this fastening. The corresponding number of cycles are unexpectedly high, however. Since the computed strains match experiments well, see figure 4.8 and the solder stress is proportional to board strain, see figure 3.12, the effects of mode shapes and frequencies should be included in the strain result automatically. One possible cause for the difference between fastenings is that when the harmonic fatigue experiments were performed, the frequency was varied between the eigenfrequency ± 1 Hz for all hole fastenings. However, a difference of 1 Hz is greater for a lower frequency. This means that a fastening with a lower frequency will be subjected to a wider interval of frequencies, and thus a lower average strain. In table

5.1 the increase in response acceleration at the peak compared to edge values is listed for all fastenings. Hole 5 has the lowest eigenfrequency and consequently the biggest increase. This effect means that the average strain will be overestimated for all fastenings, but most for hole 5. This explains part of the high strain levels of hole 5. However, if adjusting the strain of each fastening and recreating the EN-curve in figure 4.9, the relative mean absolute error decreases from 11.3 % to 10.3 %, meaning that there are more factors at play beyond this effect.

Table 5.1: Increase in response acceleration at eigenfrequency f compared to at $f \pm 1$ Hz.

Hole	Diff [%]
3	7.9
4	12
5	23
6	5.2

As mentioned in section 3.6, the eigenfrequencies of individual boards varied. At most, the measured eigenfrequency differed by 26 Hz from the experimental values presented in table 4.3. The individual eigenfrequency was always used in the vibration to failure experiment, as well as when computing the number of cycles. Thus the most obvious errors due to differing eigenfrequency were eliminated. However, the change in frequency is also indicative of a change in conditions. It is likely that these changes also affect the relationship between input acceleration and strain presented in section 4.3. A higher eigenfrequency than expected is indicative of a PCBA with higher effective stiffness. Therefore the deformation, and thus strain, should be lower for a PCBA with higher eigenfrequency. Since the relationship between acceleration and strain is based on certain conditions, the strain level is over-estimated for boards with higher eigenfrequency than expected. The opposite is true for boards with lower eigenfrequency than expected. This may contribute to the observed fastening discrepancy. For example, all but two runs for hole 5 had a higher eigenfrequency than expected, and should therefore have a slightly lower strain value than the one used. Similarly, this effect should slightly increase the strain values for all hole 6 data points, except for the one that is above the linear fit. However, for fastenings 3 and 4, no obvious pattern could be seen. For these fastenings, some points would be adjusted closer to the line and some further away from it. Therefore, this effect cannot fully explain the spread in results.

5.3 Model validation versus experiments

Unfortunately it was not possible to perform a full and rigorous validation. It would have been ideal to have another PCBA with a new shape or component placement in combination with a dummy BGA component assembled to it. In that way it would have been possible to simulate the expected lifetime and then perform a vibrate-

to-failure experiment in the same manner. This would have created a complete validation. Due to constraints in time and resources, this type of validation was not possible. Instead, the existing PCBAs were used with new hole-fastenings. This changes the relative distances between fixed points in the PCBA and the component, which can in a way be seen as a new and unknown PCBA-setup.

The validation points from the boards with new hole fastenings display a larger relative absolute error than the original data points, 26.8 % compared to 9.55 %. However, if hole fastening 51 is excluded, the relative error of the validation points is only 8.65 %. A validation error of similar magnitude as the error of the original data indicates that the spread is in part a result of individual differences between boards, rather than some error in the method.

The reason for the poor match of fastening 51 is not known. One possible explanation is the mode shape. In all standard hole fastenings, as well as the other two validation fastenings, the supports have been symmetrical around the BGA. This is not the case for fastening 51, which means that it does not get the same characteristic bowl shape at its eigenfrequency. This could mean that even if the simulated strain is correct it may not cause the same amount of damage to the solderings. If only one corner experiences the high strain levels, the rest of the component may partly compensate, thus lowering the maximum load. It was noted in the simulations that one corner of the BGA experienced significantly higher strains than the other three, which was confirmed by the experimental result. This means that only one solder ball experiences the highest stress levels, instead of four. Since this reduces the likelihood of voids or other defects to occur, it could help explain the reason why the PCBAs could sustain vibration for much longer time than expected. It should be noted that one of the PCBAs was vibrated for a significant time after the initial break, but without damage to the other three corners.

The initial validation was performed on the same type of PCBA as the material parameters were calibration for. This means that the conditions were optimal for the validation, since the calibration should have compensated for possible geometrical errors between model and reality. Therefore, using the same calibrated parameters on a complete different PCBA would likely yield worse results than the ones obtained in section 4.6.1.

As mentioned in section 4.6.2 the rule of thumb of non-linearity at deformation angles of 0.25° and higher does not hold well for the validation PCBA. This is likely due to the difference in geometry and mode shapes. Most notable is the fact that the largest deformation at the mode giving the largest strain is not located in the middle of the PCBA. The PCBAs used before validation all had a mode with a distinct bowl shape, symmetric about the middle of the board. The validation board instead experienced the largest deformation at a free edge. This is likely to allow larger deformations in a linear range. The validation board is also longer and narrower than the original boards, which might also have allowed for a larger angle. This is not considered very likely however, since the original boards were also effec-

tively of varying sizes, due to to the fixed supports at varying positions.

5.4 Applicability

The method can be applied to real projects to roughly estimate PCBA lifetime for BGA components. It only requires a CAD model of the PCBA and information about hole-fastenings to get an estimation between cycles-to-failure and vibrational level.

In the linear region, for accelerational levels that cause angle deformations below 0.25°, a function in Ansys can be used to directly give the lifetime in seconds. The functions is called *Life*. It requires an SN-curve in the engineering data for the applied material. This is the obtained EN-curve multiplied with Young's modulus for the PCB-material. The function then computes the lifetime based on the obtained stress levels in the PCB-material. The desired surface to investigate is added as input to the function together with the vibrational level. As output is a heat-map describing the lifetime over the desired surface. Here, care must be taken to avoid stress concentrations. If a stress concentration occurs in the model this will give a very short lifetime at that specific location, which also is sensitive to mesh refinement. This problem can be avoided by using the probe function to obtain the results outside of the stress concentration.

Above the linear region, the rule of thumb must be used to compute the strain based on the simulations. All data points obtained for creating the EN-curve were located in the non-linear region. Some caution must therefore be observed when the EN-curve is extrapolated into the linear region with lower accelerational levels since there may be a fatigue limit for the solders, which has not been established.

5.4.1 General design tips

Some design tips to consider when designing a PCB to withstand solder fatigue are stated here. These are tips that can be applicable for many occasions when designing a PCB and they are therefore kept as general as possible.

It is important that the supportive structure or casing and the PCBA meets the octave law. This law states that the eigenfrequencies of the casing and the PCBA should differ by at least a factor of 2. If they are too close to each other, coupling effects will play an significant role. The amplified output vibration of the casing will be the input vibration to the PCBA. The two amplifications at any one frequency are multiplied together, quickly resulting in very high strain levels.

Heavy components should be placed close to the fixed points of the PCB. Above all, they should not be placed in the center of a PCB that is fixed along its edges. It has been verified by simulations that the deformations and strain levels of the

PCBA strongly increases when a point mass is moved away from the fixing points. The adding of mass to the PCBA also shifts the natural frequencies towards lower frequencies, which is more harmful for the PCBA. For the same accelerational level, the deformations and strain levels are larger for lower frequencies. As far as it is possible, small and lightweight components should be the first choice.

It is also beneficial to stiffen the PCBA with more fixing points to shift eigenfrequencies upwards and in that way decrease the strain levels. Stiffening the PCBA with more fixing points only works if the casing can be seen as rigid in comparison to the PCBA.

Having a solder mask defined pad typically reduces the risk of complications during manufacturing. On the other hand, the microsectioning analysis in section 4.7.2 shows that the solder mask defined pad are more sensitive to forming cracks. In all cases the cracks were initiated on the solder mask defined pad while the non-solder mask defined pad showed no indication of cracks forming.

The last design tips is regarding the connections of the BGA-component to the PCB. If it is possible and the BGA component allows it, it would be desirable to not put any vital connections through the soldering points in the outer circuits. By not using the outer circuit, but still solder it to the board, the lifetime could be improved approximately eight times. Again depending on the component used, it could be possible to create some resistance monitoring over the outer circuit to send a warning to the system if the outer circuits breaks.

5.5 Relating random and harmonic vibration

The EN-curves for harmonic and random vibrations, figures 4.9 and 4.15 are plotted together in figure 5.3. As seen in this figure, the two curves do not match at all. For a given strain level, the harmonic fit predicts a number of cycles to failure over 300 times longer. Thus, this method of converting random vibration levels to harmonic vibration levels can not be said to be feasible in its current form. Since the strain value for random vibrations is chosen to be conservative a more realistic approach, such as cycle counting and damage accumulation, would only make the difference between the two results bigger. Finding a suitable method for this conversion would be a valuable addition to this result. It is possible that the Q-value used was not the correct one, or that the method of simply converting an equivalent $G_{3\sigma}$ input to a single strain level is not sound. More careful study of the relationship between random and harmonic vibrations is necessary to to develop a useful relationship.

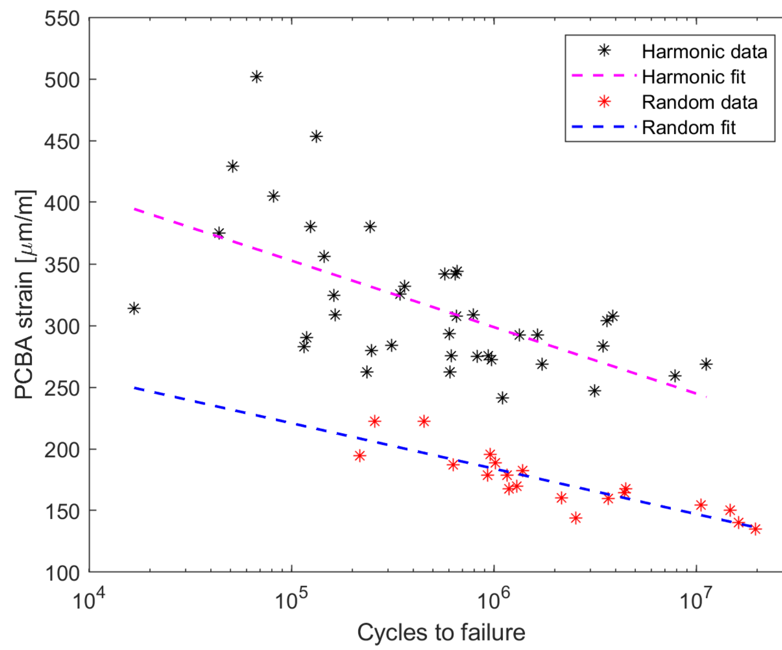

Figure 5.3: EN-curve of random vibrations converted to harmonic levels, together with original harmonic EN-curve

Bibliography

[1] Ron S. Li. “Failure Mechanisms of Ball Grid Array Packages Under Vibration and Thermal Loading”. In: *SAE Transactions* 113 (2004), pp. 767–772. ISSN: 0096736X, 25771531. URL: http://www.jstor.org/stable/44699996 (visited on 01/17/2023).

[2] Joshua a Depiver, Sabuj Mallik, and Dani Harmanto. “Solder joint failures under thermo-mechanical loading conditions – A review”. In: *Advances in Materials and Processing Technologies* 7.1 (2021), pp. 1–26. DOI: 10.1080/2374068X.2020.1751514. eprint: https://doi.org/10.1080/2374068X.2020.1751514. URL: https://doi.org/10.1080/2374068X.2020.1751514.

[3] Bhagwan D. Agarwal, Lawrence J. Broutman, and K. Chandrashekhara. *Analysis and Performance of Fiber Composites.* John Wiley & Sons, Incorporated, 2017. ISBN: 9781119390008.

[4] James C. Rautio and Serhend Arvas. “Measurement of Planar Substrate Uniaxial Anisotropy”. In: *IEEE Transactions on Microwave Theory and Techniques* 57.10 (2009), pp. 2456–2463. DOI: 10.1109/TMTT.2009.2029030.

[5] J.M. Pitarresi. “Modeling of printed circuit cards subject to vibration”. In: *IEEE International Symposium on Circuits and Systems.* 1990, 2104–2107 vol.3. DOI: 10.1109/ISCAS.1990.112213.

[6] P K Dash, M Thraza, and Babithakodavanla. “Modelling and simulation of effect of component stiffness on dynamic behaviour of printed circuit board”. In: *International Journal of Mechanical and Production Engineering Research and Development* 8 (Mar. 2018). DOI: 10.24247/ijmperdapr201834.

[7] Robin Alastair Amy, G.S. Aglietti, and Guy Richardson. “Sensitivity analysis of simplified Printed Circuit Board finite element models”. In: *Microelectronics Reliability* 49.7 (2009), pp. 791–799. ISSN: 0026-2714. DOI: https://doi.org/10.1016/j.microrel.2009.04.002. URL: https://www.sciencedirect.com/science/article/pii/S0026271409001127.

[8] Fong Wong, Pramod Malatkar, Canham Rick, et al. “Vibration Testing and Analysis of Ball Grid Array Package Solder Joints”. In: Jan. 2007, pp. 373 –380. ISBN: 1-4244-0985-3. DOI: 10.1109/ECTC.2007.373825.

[9] Uday H. Kalyani and Mark Wylie. “Modal finite element analysis of PCBs and the role of material anisotropy”. In: *Vibroengineering PROCEDIA* 32 (June 2020), pp. 75–80. DOI: 10.21595/vp.2020.21446. URL: https://doi.org/10.21595/vp.2020.21446.

[10] Thomas Abrahamsson. *Structural Dynamics and Linear Systems Compute, Test, Calibrate and Validate*. Chalmers University of Technology, 2019.

[11] Dave S. Steinberg. *Vibration Analysis for Electronic Equipment*. 3rd ed. John Wiley & Sons, 2000. ISBN: 978-0-471-37685-9. URL: https://app.knovel.com/hotlink/toc/id:kpVAEEE001/vibration-analysis-electronic/vibration-analysis-electronic.

[12] Norman E. Dowling. *Mechanical behavior of materials: engineering methods for deformation, fracture, and fatigue*. 4th ed. Pearson Education, 2012. ISBN: 0-273-76455-1.

[13] Stefan Keil. *Technology and Practical Use of Strain Gages - With Particular Consideration of Stress Analysis Using Strain Gages*. John Wiley & Sons, Incorporated, 2017. ISBN: 978-3-433-03138-4.

[14] Sam Lau, Joey Gonzalez, and Deb Nolan. "Bootstrapping for Linear Regression (Inference for the True Coefficients)". In: *Principles and Techniques of Data Science*. 2020. URL: https://www.samlau.me/test-textbook/ch/18/hyp_regression.html#bootstrapping-for-linear-regression-inference-for-the-true-coefficients.

[15] Sufyan Azam and Alex Fragoso. "Experimental and Numerical Simulation Study of the Vibration Properties of Thin Copper Films Bonded to FR4 Composite". In: *Applied Sciences* 10 (July 2020), p. 5197. DOI: 10.3390/app10155197.

[16] Henrik Sönnerlind. "What Is Geometric Nonlinearity?" In: *COMSOL Blog* (2015). URL: https://www.comsol.com/blogs/what-is-geometric-nonlinearity/ (visited on 04/27/2023).

DEPARTMENT OF MECHANICS AND MARITIME SCIENCES
CHALMERS UNIVERSITY OF TECHNOLOGY
Gothenburg, Sweden
www.chalmers.se

CHALMERS
UNIVERSITY OF TECHNOLOGY